Journal of Pharmaceutical Analysis 14 (2024) 100977

Contents lists available at ScienceDirect

Journal of Pharmaceutical Analysis

journal homepage: www.elsevier.com/locate/jpa

Original article

Xianling Lianxia formula improves the efficacy of trastuzumab by enhancing NK cell-mediated ADCC in HER2-positive BC

Feifei Li [a, b], Youyang Shi [a], Mei Ma [c], Xiaojuan Yang [a], Xiaosong Chen [d, ***], Ying Xie [b, **], Sheng Liu [a, b, *]

[a] Department of Breast Surgery, Longhua Hospital, Shanghai University of Traditional Chinese Medicine, Shanghai, 200030, China
[b] Institute of Chinese Traditional Surgery, Longhua Hospital, Shanghai University of Traditional Chinese Medicine, Shanghai, 200030, China
[c] Institute of Toxicology, School of Public Health, Lanzhou University, Lanzhou, 730000, China
[d] Department of General Surgery, Comprehensive Breast Health Center, Ruijin Hospital, Shanghai Jiao Tong University School of Medicine, Shanghai, 200001, China

ARTICLE INFO

Article history:
Received 12 October 2023
Received in revised form
8 February 2024
Accepted 8 April 2024
Available online 10 April 2024

Keywords:
HER2-positive breast cancer
Traditional chinese medicine
Trastuzumab
NK cell
ADCC effect

ABSTRACT

Trastuzumab has improved survival rates in human epidermal growth factor receptor 2 (HER2)-positive breast cancer (BC), but drug resistance leads to treatment failure. Natural killer (NK) cell-mediated antibody-dependent cell cytotoxicity (ADCC) represents an essential antitumor immune mechanism of trastuzumab. Traditional Chinese medicine (TCM) has been used for centuries to treat diseases because of its capacity to improve immune responses. Xianling Lianxia formula (XLLXF), based on the principle of "strengthening body and eliminating toxin", exhibits a synergistic effect in the trastuzumab treatment of patients with HER2-positive BC. Notably, this synergistic effect of XLLXF was executed by enhancing NK cells and ADCC, as demonstrated through *in vitro* co-culture of NK cells and BC cells and *in vivo* intervention experiments. Mechanistically, the augmented impact of XLLXF on NK cells is linked to a decrease in cytokine inducible Src homology 2 (SH2) containing protein (*CISH*) expression, which in turn activates the Janus kinase 1 (JAK1)/signal transducer and activator of transcription 5 (STAT5) pathway. Collectively, these findings suggested that XLLXF holds promise for enhancing NK cell function and sensitizing patients with HER2-positive BC to trastuzumab.

1. Introduction

Breast cancer (BC) is the most prevalent malignancy among women globally [1]. Human epidermal growth factor receptor 2 (HER2)-positive BC is known for its aggressive phenotype and high recurrence rates due to HER2 amplification and overexpression [2]. Trastuzumab functions by binding to HER2 receptors and impeding their homodimerization, thereby demonstrating high efficacy in inhibiting HER2-positive BC [3,4]. However, treatment resistance, metastasis [5], and disease progression [6] remain significant challenges for patients with HER2-positive BC [7]. Moreover, patients with poor trastuzumab efficacy have a limited survival benefit from alternative anti-HER2 therapies, leading to high mortality rates. Therefore, there is a continued effort to explore solutions that can enhance the effectiveness of trastuzumab in these patients [8].

Trastuzumab is an immunoglobulin G (IgG) antibody that is capable of inducing the release of cytotoxic particles by natural killer (NK) cells in HER2-positive BC through the mechanism of antibody-dependent cell-mediated cytotoxicity (ADCC) [9]. However, ADCC is suppressed in trastuzumab-resistant HER2-positive BC tumor tissues, which highlights the importance of understanding the process of ADCC and identifying breakthrough points [10].

The process of ADCC is initiated when the antigen-binding fragment (Fab) region of trastuzumab specifically binds to HER2 on the surface of BC cells. NK cells then engage with the fragment crystalline (Fc) region of trastuzumab through their Fc gamma receptor (FcγR) [11,12]. Subsequently, NK cells release toxic granules such as perforin and granzyme B to exhibit the cytotoxicity effect. Considering the pivotal role of NK cells in ADCC, enhancing NK cells is of great importance for improving the therapeutic effect of trastuzumab in HER2-positive BC.

NK cell function is regulated through a dynamic balance of inhibitory and activating receptors. The inhibitory receptors of NK

* Corresponding author. Department of Breast Surgery, Longhua Hospital, Shanghai University of Traditional Chinese Medicine, Shanghai, 200030, China.
** Corresponding author.
*** Corresponding author.
E-mail addresses: chenxiaosong0156@hotmail.com (X. Chen), sherryyx36@shutcm.edu.cn (Y. Xie), lshtcm@163.com (S. Liu).

https://doi.org/10.1016/j.jpha.2024.100977

cells, mainly killer cell immunoglobulin-like receptors (KIRs) and NK group 2 member A (NKG2A), can bind to major histocompatibility complex class I (MHC-I) molecules and transmit inhibitory signals [13]. Normal healthy cells express an adequate number of MHC-I molecules, which "silence" NK cells and prevent them from being "mistakenly killed." NKp46 and NKG2D are key activating receptors on the surface of NK cells. Optimizing NKp46 has emerged as a promising strategy for enhancing cancer immunotherapy by promoting NK cell activation and cytotoxicity and inhibiting tumor growth [14]. Studies using an NKp46-knockout mouse model have suggested that this receptor is vital for controlling cancer metastasis [15]. Researchers have developed NK cell engagers that simultaneously target NKp46, CD16, and tumor antigens, resulting in increased numbers of tumor-infiltrating NK cells, enhanced NK cell activation, ADCC, and improved antitumor immunity [16]. Additionally, targeting the NKG2D−NKG2DL axis through immunotherapy approaches has shown promise in enhancing the antitumor effects of NK cells and $CD8^+$ T cells [17]. BI836858, a fully human, Fc-engineered, anti-CD33 antibody, which opsonizes acute myeloid leukemia cells, significantly induces autologous and allogeneic NK-cell degranulation and ADCC. However, when NKG2DL receptor is blocked using antibodies, BI836858-mediated ADCC is significantly decreased [18]. These studies revealed that NKp46 and NKG2D play a crucial role in the process of ADCC.

In modern times, traditional Chinese medicine (TCM) has been widely used as adjuvant therapy for cancer treatment in East Asia, and its immunoregulation mechanism is under extensive study. TCM formulas are formed based on TCM theory concerning multiple aspects of the disease. In TCM theory, patients with BC, especially those after surgery and chemotherapy, exhibit deficiency and stagnation of Qi while the tumor itself is characterized as the accumulation of "phlegm and poison" in the breast. Accordingly, Xianling Lianxia formula (XLLXF) is composed of Epimedii Folium (XLP), Codonopsis Radix (DS), and Poria (FL), which serve as tonics to strengthen Qi and resolve phlegm. Curcumae Rhizoma (EZ) mainly acts to promote the movement of Qi and blood. Scutellaria Barbata (BZL) and Prunellae Spica (XKC) exhibit abilities in resolving phlegm, detoxifying toxins, and dispersing nodules. Clinical evidence has demonstrated the efficacy of XLLXF therapy in improving the three-year disease-free survival (DFS) rate in patients diagnosed with HER2-positive BC [19].

The immunomodulatory effects of the XLLXF components have been reported. In a melanoma mouse model, icariside I upregulates lymphocyte subsets in the peripheral blood, including $CD4^+$ and $CD8^+$ T cells, as well as NK and natural killer T cell (NKT) cells [20]. In triple-negative BC mice, treatment with icariin significantly increases the proportion of tumor-infiltrating $CD4^+$ and $CD8^+$ T cells [21]. Scutellaria extract and wogonin reverse tumor-mediated immunosuppression by inhibiting transforming growth factor-β (TGF-β)-1 secretion in gliomas [22]. Steamed Codonopsis lanceolata has been shown to increase the levels of serum interferon-gamma (IFN-γ), tumor necrosis factor-alpha (TNF-α), interleukin (IL)-6, and IL-2, thereby improving immune function and inhibiting the growth of tumors *in vivo* [23].

Here, we conducted a five-year follow-up on patients with HER2-positive BC to evaluate their long-term benefits based on previous clinical research, which ensured a balanced baseline between the two groups by propensity score matching (PSM) prior to assessment. Clinical and experimental findings confirmed the ability of XLLXF to enhance the therapeutic efficacy of trastuzumab by augmenting NK cell activity. Mechanistically, we discovered that XLLXF may exert its promoting effect on NK cell activity and ADCC effect by suppressing cytokine inducible Src homology 2 (SH2) containing protein (*CISH*) expression. Additionally, we conducted functional validation of the potential active components in XLLXF, which provides a clear direction for future investigations. These findings contribute to the development of effective components that enhance NK cell activity and offer a promising therapeutic strategy for tumor immunotherapy in HER2-positive BC.

2. Materials and methods

2.1. Cohort study

Cohort 1 and cohort 2 of patients with HER2-positive BC were recruited between May 2014 and May 2018, from Longhua Hospital affiliated to Shanghai University of Traditional Chinese Medicine (Shanghai, China) and Ruijin Hospital affiliated to Shanghai Jiaotong University School of Medicine (Shanghai, China), respectively. HER2-positive BC was confirmed by pathology. In total, 844 patients who were prescribed trastuzumab as their targeted therapy were included, whose age range was 18−80 years. Cohort 1 comprised 168 patients from Longhua Hospital who received trastuzumab and XLLXF within one year of surgery. Cohort 2 comprised 676 patients from Ruijin Hospital who received trastuzumab after surgery. A retrospective study on these cohorts was conducted to explore whether XLLXF enhances trastuzumab efficacy to prolong DFS. Patients with advanced BC or multiple primary cancers were excluded from the study, as were those with severe pre-existing conditions or who were receiving other targeted drugs besides trastuzumab. XLLXF treatment was restricted to that initiated within a year after surgery and lasted for over two years. A schematic of the patient selection process is displayed in Fig. 1A. After screening and PSM, 82 patients from cohort 1 and 274 patients from cohort 2 were subjected to analysis. All patients were followed up for a period of five years post-surgery. This study was ethically approved by the Medical Ethics Committee of Longhua Hospital, Shanghai University of Traditional Chinese Medicine (Approval No.: 2021LCSY043).

2.2. Infiltrating immune cell estimation from transcriptome analysis

Gene expression data of HER2-positive BC were obtained from the Gene Expression Omnibus (GEO) database, including GSE44272, GSE50948, and GSE66305. To analyze the correlation between infiltrating immune cells and trastuzumab response, we excluded data from patients treated with other drugs besides trastuzumab and from those without responding records. Normalized RNA-seq data from the remaining 156 patients were used for further analysis. To estimate the fraction of immune cell infiltrating in tumors, we uploaded the obtained gene expression data to the online tool of xCell (https://xcell.ucsf.edu/). This deconvolution tool uses mathematical algorithms to determine the proportions of different cell types present in a mixed population of cells by comparing the expression levels of cell-specific marker genes to reference gene expression for each cell type.

2.3. Peripheral blood collection from patients

Peripheral blood samples were collected from patients with HER2-positive BC who were recruited from Longhua Hospital affiliated to Shanghai University of Traditional Chinese Medicine. All patient donors signed an approved informed consent form before providing blood samples. Patients aged between 18 and 80 years, who had previously received trastuzumab-targeted therapy, were eligible to voluntarily participate in the study. Peripheral blood samples were collected from the patients before and six months after taking XLLXF. $CD56^+CD16^+$ NK cell composition of the blood was determined by flow cytometry analysis.

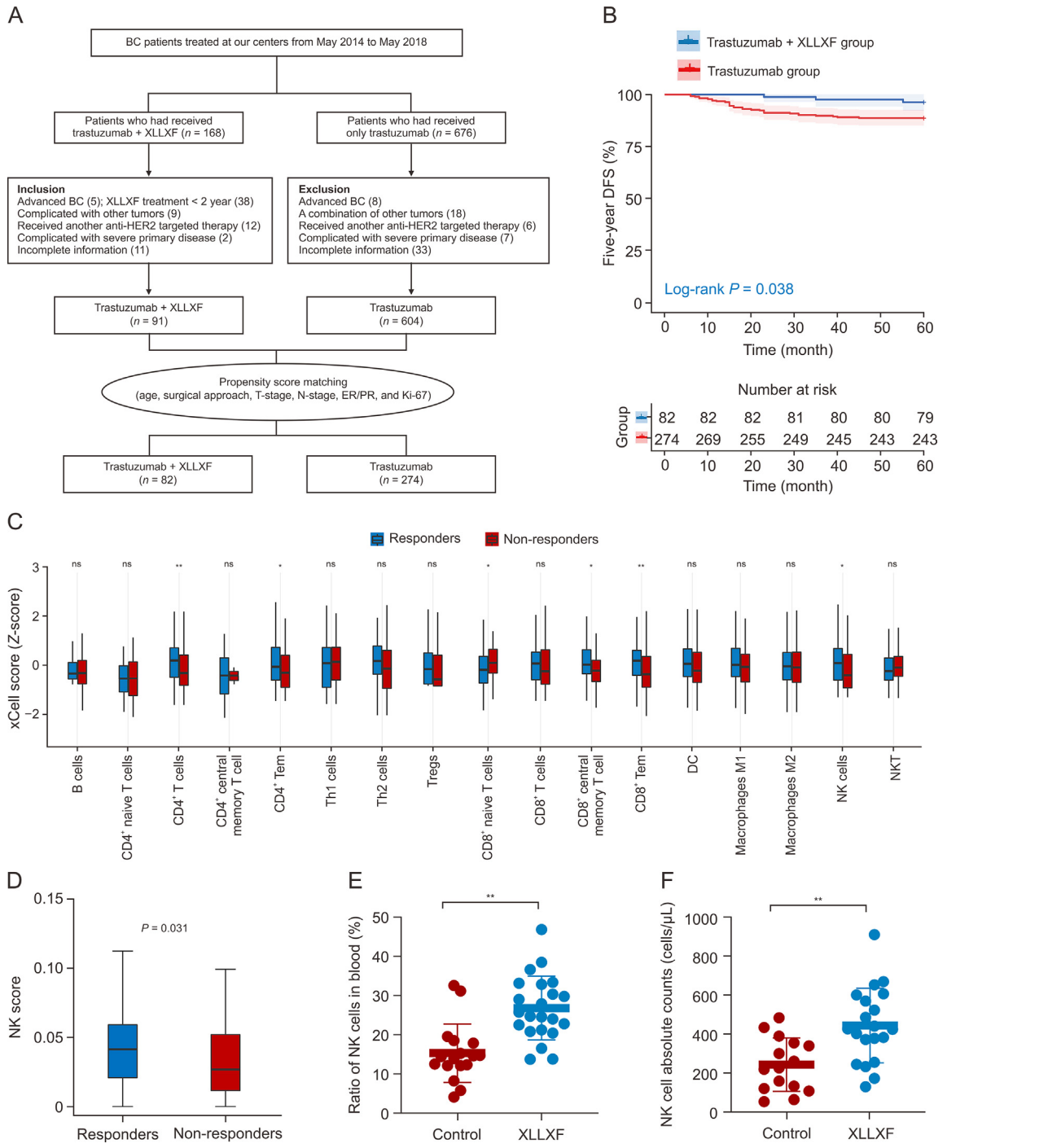

Fig. 1. Xianling Lianxia formula (XLLXF) synergizes with trastuzumab to improve the five-year disease-free survival (DFS) in patients with human epidermal growth factor receptor 2 (HER2)-positive breast cancer (BC). (A) Patients recruitment flowchart of cohort study. (B) Kaplan-Meier plots for five-year DFS between the trastuzumab plus XLLXF group ($n = 82$) and the trastuzumab group ($n = 274$). (C, D) Bioinformatics analysis: tumor gene expression data obtained from Gene Expression Omnibus (GEO) database demonstrated the degree of immune cell infiltration (C), and further analysis showed that trastuzumab responders exhibited substantially higher levels of natural killer (NK) cell infiltration compared with the non-responders (D). in trastuzumab responders and non-responders groups. (E, F) NK cells proportion (E) and absolute counts (F) in peripheral blood samples of patients with HER2-positive BC. Their peripheral blood samples were collected before (control) and six months after taking XLLXF (XLLXF). $^{*}P < 0.05$, and $^{**}P < 0.01$. T-stage: tumor stage; N-stage: node stage; ER: estrogen receptor; PR: progesterone receptor; Tem: effector memory T cell; Tregs: regulatory T cells; DC: dendritic cell; NKT: natural killer T cell.

2.4. XLLXF preparation

The preparation of XLLXF was consistent with the previously published literature [24]. In general, DS (12 g), FL (12 g), XLP (15 g), XKC (9 g), EZ (30 g), and BZL (30 g) were boiled in distilled water. The final decoction was filtered, concentrated, and freeze dried to obtain the XLLXF extract at a yield of 29.23% (*m*/*m*, dried extract/crude herbs). All herbs were provided by Shanghai Kang Qiao Chinese Cut Crude Drug Co., Ltd. (Shanghai, China) and identified by Wuxi Apptec Co., Ltd. (Shanghai, China). Morphological, microscopic, and phytochemical identification were performed in accordance with the Pharmacopoeia of the People's Republic of China (2015 edition).

2.5. XLLXF and serum samples for ultra-high-performance liquid chromatography-Q Exactive-tandem mass spectrometry (UPLC-QE-MS) analysis

Chemical constituents of XLLXF and serum samples were analyzed by UPLC-QE-MS/MS. The optimal quantity of XLLXF freeze-dried powder was dissolved in methanol to obtain a concentration of 0.00635 g/mL. After filtration through a 0.22-μm filter membrane, the solution was injected in increments of 2 μL at a time. Medicated and control blood samples were collected from BALB/c nude mice that were orally administered XLLXF (10.52 mg/kg twice a day for three days) and distilled water, respectively. Blood samples were collected at 1 and 2 h post-final gavage and allowed to rest at room temperature for 1 h until solidification. The samples were then centrifuged at 3,000 rpm for 10 min, and the upper layer of serum was collected. Methanol was added to the serum samples three times, mixed, and centrifuged at 12,000 rpm for 20 min. The supernatant was dried with nitrogen gas. The remaining residue was dissolved in 50 μL of methanol and centrifuged again at 12,000 rpm for 20 min. The supernatant was then used for UPLC-QE-MS/MS analysis. MS was performed using a Thermo-Obritrap-QE (Thermo Fisher Scientific Inc., Waltham, MA, USA) instrument, and the following operating parameters were used: spray voltage, 3800 V; capillary temperature, 320 °C; auxiliary gas heater, 350 °C; sheath gas flow rate, 35 arb; auxiliary gas flow rate, 8 arb; super-lens radio frequency level, 50; mass range, *m*/*z* 1000−1200; full MS resolution, 70,000; and MS/MS resolution, 17,500.

2.6. Cell culture

Human HER2-positive BC cells SK-BR-3 and JIMT-1 were purchased from National Collection of Authenticated Cell Cultures (Shanghai, China). Cells were grown in Dulbecco's modified Eagle's medium (DMEM; Gibco, Waltham, MA, USA) supplemented with 10% fetal bovine serum (FBS; Gibco) and 1% penicillin/streptomycin in a humidified atmosphere with 5% CO_2 at 37 °C.

2.7. Cultivation and identification of primary human NK cells

Fresh peripheral blood was collected from healthy volunteers with written informed consent. Peripheral blood NK cells were isolated using a Human NK Cell Enrichment Set-DM kit (BD Biosciences, Franklin Lakes, NJ, USA) and expanded using an NK Cell Robust Expansion kit (Fujian Sany Hematopoietic Technology Co., Ltd., Xiamen, China) according to the manufacturer's instructions. Flow cytometry was employed to assess the purity and amplification of NK cells by analyzing the percentage of CD3, CD56, and CD16 when NK cells were cultivated up to day 14. The activity of NK cells was estimated by analyzing the percentage of CD107a, NKp46, and NKG2D. Anti-human CD3-fluorescein isothiocyanate (FITC), anti-human CD56-allophycocyanin (APC), anti-human CD16-phycoerythrin (PE), anti-human NKp46-peridinin chlorophyll protein (PerCP), anti-human CD107a-PE, and anti-human NKG2D-peridinin chlorophyll protein complexed with cyanine 7 (PECy7) were purchased from BioLegend Co., Ltd. (San Diego, CA, USA). The experimental protocols were conducted following the guidelines outlined in Ref. [25].

2.8. Animal models

Animals used were permitted by the Ethical Review Board of Shanghai University of Traditional Chinese Medicine (Approval No.: PZSHUTCM211115006). Female BALB/c nude mice (six weeks) of specific pathogen free (SPF) grade were procured from Shanghai Slake Experimental Animal Co., Ltd. (Shanghai, China). All mice were housed in pathogen-free conditions with free access to water and feed in a 12-h light/12-h dark cycle. Subsequently, 5×10^6 JIMT-1 cells were injected into the left flank of each nude mouse, which was suspended in phosphate-buffered saline (PBS) mixed with matrigel in a 1:1 vol ratio. The tumor volume was periodically measured using the following formula: volume $= 0.5 \times$ length $\times$ width^2. Treatment was initiated when the tumor size reached 100 mm^3. XLLXF was orally administered via gavage at a dose of 5.26 mg/kg once daily, whereas trastuzumab was injected intraperitoneally at a dose of 5 mg/kg twice weekly. The mice were euthanized after four weeks of continuous administration.

2.9. Depletion of NK cells by asialo GM-1 (ASGM-1) antibody

To chronically deplete NK cells *in vivo*, we intraperitoneally injected tumor-bearing mice with 25 μL of anti-ASGM-1 antibody (BioLegend Co., Ltd.) or IgG control every four days, starting one day prior to other treatments. Meanwhile, XLLXF was orally administered via gavage once daily at a dose of 5.26 mg/kg, whereas trastuzumab was injected intraperitoneally twice weekly at a dose of 5 mg/kg. At the end of the experiment, tumors were excised from euthanized mice for further analysis. Spleens were also harvested and prepared into single-cell suspensions. In BALB/c mice, CD49b$^+$ marks NK cells, similar to NK1.1$^+$ in other mouse strains such as C57BL, FVB/N, and NZB. Depletion of NK cells was confirmed via flow cytometry by staining splenocytes with an antibody against CD49b.

2.10. In vivo evaluation of primary human NK cells

The JIMT-1 xenograft mouse model was established as described above in Section 2.8. Human NK cells were cultivated and verified as described in Section 2.7. When tumor volume reached 100 mm^3, each mouse received an intravenous injection of 1×10^7 primary human NK cells alone or combined with trastuzumab (5 mg/kg) on days 1, 5, 9, 13, 17, and 20. Trastuzumab (5 mg/kg) was injected intraperitoneally twice a week. NK cells were pretreated with control or 100 μg/mL XLLXF for 48 h before injection. Tumor size was monitored to evaluate the effect of different treatments.

2.11. Flow cytometry analysis of splenic NK cells

Fresh mouse spleen tissues were processed into single-cell suspensions. Surface staining and intracellular staining were performed according to the manual of the fixation and permeabilization buffer (BioLegend Co., Ltd.). Surface antibodies were stained before fixation, and intracellular antibodies were stained after fixation and permeabilization. The gating method is provided in Fig. S1. The anti-mouse NKp46-BV605, anti-mouse NKG2D-BV711, anti-mouse CD45-BV421, anti-mouse CD49b-PECy7, and anti-mouse perforin-APC were purchased from BioLegend Co., Ltd.. The anti-mouse granzyme B-PE, anti-mouse CD11b-PECy5.5, and anti-mouse CD107a-AF488 were purchased from eBioscience Co., Ltd. (Waltham, MA, USA).

2.12. Immunohistochemistry

Tumor tissues were collected at each experimental endpoint, formalin-fixed for 24 h, and embedded in paraffin after dehydration. Sections were cut to a thickness of 4 μm, and slides were deparaffinized and rehydrated, with antigens being retrieved in citrate buffer for 13 min at high heat (−95 °C). Slides were then subjected to a 30 min antigen retrieval step in citrate buffer (pH 6.0) and blocked in 0.1% bovine serum albumin (BSA) for 30 min at room

temperature. The corresponding antibodies were applied, and the slides were incubated overnight. A secondary antibody was introduced and incubated for 1 h at room temperature. The slides were developed with the Dako liquid 3,3'-diaminobenzidine tetrahydrochloride (DAB) + substrate chromogen system.

2.13. Terminal dexynucleotidyl transferase-mediated dUTP nick-end labeling (TUNEL) assay

TUNEL assay was conducted using the TUNEL Cell Apoptosis Detection Kit (Roche, Shanghai, China) in accordance with the manufacturer's instructions. In brief, the sliced samples were sequentially incubated with proteinase K, TUNEL detection solution, and converter-peroxidase. Finally, cell nuclei were stained with 4',6-diamidino-2-phenylindole (DAPI), and the TUNEL-positive cells were visualized using a fluorescence microscope (Pannoramic DESK, 3DHISTECH Ltd., Budapest, Hungary).

2.14. Immunofluorescence staining

Paraffin-embedded specimens of HER2-positive BC tissues underwent a series of preparation steps starting with washing, fixation, permeabilization, and blocking utilizing goat serum. Subsequently, corresponding specific antibodies were applied to the tissue specimens and left to incubate overnight at 4 °C. The specimens underwent further incubation with fluorescent secondary antibodies in a dark environment for 1 h at 37 °C. To counterstain the nuclei and mount the tissue specimens, we utilized aqueous mounting medium with Fluoroshield (Beyotime Biotechnology, Shanghai, China) with DAPI. Fluorescence was then observed using a confocal laser scanning microscope.

2.15. Western blot

Proteins isolated from cells or tissues were separated (25−30 mg for each sample) using sodium dodecyl sulfate-polyacrylamide gel electrophoresis (SDS-PAGE) gels and then transferred to polyvinylidene difluoride membranes (Millipore, Billerica, MA, USA). Following blocking with 5% nonfat milk, the primary antibody (1:1000) was added to each membrane for incubation for 24 h at 4 °C. The membranes were incubated with a 1:2000 dilution of an horseradish peroxidase (HRP)-conjugated secondary antibody at 25 °C for 1 h. Following incubation with an enhanced chemiluminescence plus reagent, the blots were visualized using an Image Quant LAS 4000 mini system (GE Healthcare, Chicago, IL, USA). Chemifluorescence was quantified using ImageJ software (Bio-Rad Laboratories, Hercules, CA, USA). The rabbit polyclonal antibody (pAb) of KLRK1, NCR1, factor-associated suicide (FAS), perforin, human leucocyte antigen-G (HLA-G), KIR2DL4, KLRC1, factor-associated suicide ligand (FASL), and goat anti-rabbit secondary antibody were purchased by ABclonal Technology Co., Ltd. (Wuhan, China). The granzyme B, β-actin, and glyceraldehyde-3-phosphate dehydrogenase (GAPDH) antibody were purchased by Proteintech Group, Inc. (Wuhan, China).

2.16. Enzyme-linked immunosorbent assay (ELISA)

Levels of IL2, IFN-γ, IL15, and TGF-α in the cell culture supernatant and serum samples were quantified using commercially available ELISA kits (Shanghai Enzyme-linked Biotechnology Co., Ltd., Shanghai, China). The conditioned sample was added to an ELISA kit plate, which had been precoated with a specific antibody. A biotinylated secondary antibody was then introduced. 3,3',5,5'-tetramethylbenzidine was added, incubated at room temperature, and protected from light for 5−30 min until a dark blue shade developed in the wells. To terminate the reaction, 100 μL/well of stop solution was quickly introduced. Absorbance was measured at 450 nm using a microplate reader (BioTek Instruments, Inc., Winooski, VT, USA). The protein concentration was normalized to the relative absorbance rate of the standard and expressed as mean ± standard deviation (SD).

2.17. ADCC assay

ADCC was analyzed by co-culturing primary human NK cells (XLLXF pre-treatment for 48 h or not) with SK-BR-3/JIMT-1 cell lines at an effector-to-target (E:T) ratio ranging from 3:1 to 10:1. The SK-BR-3/JIMT-1 target cells were loaded with carboxyfluorescein succinimidyl ester (CFSE; eBioscience Co., Ltd.). In the co-culture system, trastuzumab (2.7 μM) was added together. After 4 h of co-culture, cytotoxicity was quantified by calculating the percentage of dead cells (APC-live/dead fixable aqua dead cell stain kit; eBioscience Co., Ltd.) in all target cells, or viability of target cells were measured by Cell Counting Kit-8 (CCK-8; Beyotime Biotechnology) assay.

2.18. Isolation of splenic NK cells in tumor-bearing mice

NK cells of the spleen were purified by negative magnetic selection using an NK Cell Isolation Kit (Miltenyi, Bergisch-Gladbach, Germany) following the manufacturer's instructions. In general, spleen was obtained from mice, and a single-cell suspension was prepared. NK cells were enriched by depleting non-NK cells (i.e., T cells, dendritic cells, B cells, granulocytes, macrophages, and erythroid cells). The purity of isolated NK cells was determined by flow cytometry.

2.19. Transcriptome

Splenic NK cells were treated with Trizol to extract RNA, which was subsequently subjected to RNA sequencing (RNA-seq) using the Illumina Novoseq platform by Sangon Biotech (Shanghai) Co., Ltd. (Shanghai, China). Differentially expressed sequence (DESeq) was employed for gene analysis of significant differences, utilizing fold change (FC) values to depict the differential gene expression. Differentially expressed genes (DEGs) were screened with a cutoff of $|FC| > 1.2$ and $P < 0.05$. Enrichment analysis of the Kyoto Encyclopedia of Genes and Genomes (KEGG) was carried out through utilization of the R cluster profile 3.12.0 package.

2.20. Establishment of low-expressing CISH primary NK cells

The small interfering RNA (siRNA)-RFect mixture was prepared by diluting 30 pmol siRNA (Gema (Shanghai) Co., Ltd., Shanghai, China) and 3 μL of RFect reagent (Changzhou Bio-generating Biotechnologies Co., Ltd., Changzhou, China) with 100 μL of serum-free medium. About 100 μL of the mixture was added to the culture wells containing 0.5 mL of cultured cells, which were under complete medium culture. RNA and total protein were extracted after 48 and 72 h, respectively. The transfection efficiency was determined via reverse transcription-polymerase chain reaction (RT-PCR) and Western blot.

2.21. RT-PCR assay

Total RNA from NK cells was extracted and purified utilizing Trizol reagent (Invitrogen, Carlsbad, CA, USA) and the RNA concentration was measured to ensure proper processing. Reverse transcription of the synthesized complementary DNA (cDNA) was performed with a ReverTra Ace qPCR RT Kit (Accurate

Biotechnology, Shanghai, China). The resulting cDNA was subjected to real-time PCR for one cycle at 95 °C for 60 s, followed by up to 40 cycles of 95 °C for 15 s, 60 °C for 15 s, and 72 °C for 45 s with SYBR Green Master Mix (Accurate Biotechnology). The messenger RNA (mRNA) level was quantified with the QuantStudio 3 Real-Time PCR system (Applied Biosystems, Foster City, CA, USA). The FC in the expression of the detected genes was calculated with the $2^{-\Delta\Delta C_T}$ method.

2.22. CCK-8 assay

The cell viability was detected by CCK-8 assay (Beyotime Biotechnology). In brief, cells were prepared into a single-cell suspension (1×10^5 cells/mL) and seeded into 96-well plates (100 μL/well). The culture medium contained various conditions of intervention. After 24 h, 10 μL of CCK-8 working solution was added to incubate at 37 °C for 12 h. Optical density (OD) was detected at 490 nm with a microplate reader (BioTek Instruments, Inc.).

2.23. Statistical analysis

Statistical analysis was performed utilizing R 4.0.3 and SPSS 25.0 softwares. PSM was performed using nearest-neighbor matching through the "matchit" package and logistic regression. Survival curves were generated using the "survival" and "survminer" packages. Differences in survival rates between groups were assessed via the log-rank test. Continuous data were presented as mean ± SD. The independent samples *t*-test was applied for normally distributed data, whereas the rank-sum test was used for non-normally distributed data. Count data were summarized as frequency and composition ratio (%), and intergroup comparisons were made using the Chi-square test. If the expected value was below 5, a continuous corrected Chi-square test was utilized. Fisher exact probability calculation was employed when the predicted value was less than 1 or the sample size *n* was less than 40. One-way analysis of variance (ANOVA) with least significant difference (LSD) post-hoc testing was performed for comparison among groups with homogeneous variances. The Games-Howell test was applied when variances were not homogeneous. A *P*-value less than 0.05 indicated statistical significance in all tests.

3. Results

3.1. XLLXF synergizes with trastuzumab to improve the five-year DFS in patients with HER2-positive BC

To verify the synergistic effect of XLLXF with trastuzumab on inhibiting HER2-positive BC, a retrospective study was conducted to analyze the DFS rate for five years after surgery using two cohorts, namely, cohort 1 who received trastuzumab and XLLXF within 1 year of surgery from Longhua Hospital Affiliated to Shanghai University of Traditional Chinese Medicine and cohort 2 who received trastuzumab after surgery from Ruijin Hospital affiliated to Shanghai Jiaotong University. In total, 844 patients with HER2-positive BC were included from 2014 to 2018 and received clinical follow-up for five years. After the screening, 695 patients were determined to be eligible for the analysis (Fig. 1A). Of these patients, 91 patients were treated with trastuzumab plus XLLXF, whereas 604 patients were treated with trastuzumab alone. After PSM to balance the two groups with respect to age, surgical approach, tumor stage (T-stage), node stage (N-stage), hormone receptor status, and Ki-67 status, 82 patients in the trastuzumab plus XLLXF group and 274 patients in the trastuzumab group were matched (Tables S1 and S2). In patients with HER2-positive BC, compared with those treated with trastuzumab alone, treatment with trastuzumab plus XLLXF could improve the five-year DFS by 7.6% (96.3% vs. 88.7%, log-rank $P = 0.038$; Fig. 1B and Table S3). Our clinical results indicated that XLLXF could enhance the efficacy of trastuzumab on HER2-positive BC treatment.

3.2. Trastuzumab efficacy is positively correlated with the degree of NK cell infiltration

To verify the importance of immune cell infiltration in trastuzumab treatment, we obtained complete sample information of 156 patients with HER2-positive BC from the GEO database, who were treated with trastuzumab alone as targeted therapy. On the basis of the objective remission criteria, patients categorized as complete response and partial response were considered as responders, whereas those with stable disease and progressive disease were defined as non-responders (Table S4). The infiltration of immune cells was determined by the single-sample gene set enrichment analysis (ssGSEA)-based enrichment scores for each cell type signature. Responders had higher infiltration levels of $CD4^+$ T cells, $CD4^+$ effector memory T cell (Tem), $CD8^+$ central memory T cell, $CD8^+$ Tem, and NK cells than non-responders, whereas $CD8^+$ naïve T cells were comparatively lower (Fig. 1C). Given the important role of NK cells in trastuzumab-targeted therapy, further analysis showed that trastuzumab responders exhibited substantially higher levels of NK cell infiltration compared with the non-responders ($P = 0.031$; Fig. 1D).

3.3. XLLXF increases NK cell levels in the peripheral blood of patients with HER2-positive BC

Given that XLLXF has been shown to enhance trastuzumab efficacy in HER2-positive BC, while NK cells are important for trastuzumab response, we sought to investigate whether XLLXF affects NK cells in patients with HER2-positive BC. Clinical data revealed a significant increase in the proportion and absolute count of NK cells in peripheral blood of patients with HER2-positive BC after six months of XLLXF treatment (Figs. 1E and F and Table S5).

3.4. XLLXF synergistically inhibits tumor growth with trastuzumab in HER2-positive BC-bearing mice

Tumor recurrence and metastasis in HER2-positive BC is associated with trastuzumab resistance, which highlights the urgent need for sensitizers in the treatment of patients with advanced HER2-positive BC. We demonstrated the potential of XLLXF to enhance trastuzumab efficacy in patients with HER2-positive BC and its correlation with increased NK cells. To address whether XLLXF sensitizes trastuzumab in resistant HER2-positive BC and further investigate its mechanism regarding NK cells, we established a trastuzumab-resistant model of JIMT-1 cell xenograft in BALB/c nude mice, which have a low number of peripheral T cells but high activity of NK cells (Fig. 2A). Resistance to trastuzumab was developed when the tumor size exceeded 100 mm^3 [26,27]. After four weeks of continuous administration, XLLXF exhibited a significant inhibitory effect on tumor growth. Notably, the trend of tumor growth, volume, and weight in the combination group was significantly lower than that in the model group (Figs. 2B–D). XLLXF demonstrated a favorable safety profile as indicated by the levels of alanine aminotransferase (ALT), aspartate aminotransferase (AST), blood urea nitrogen (BUN), and creatinine (Cr) being within the normal ranges (Fig. S2). Additionally, immunohistochemistry (IHC) results showed a decreased expression of Ki-67, a

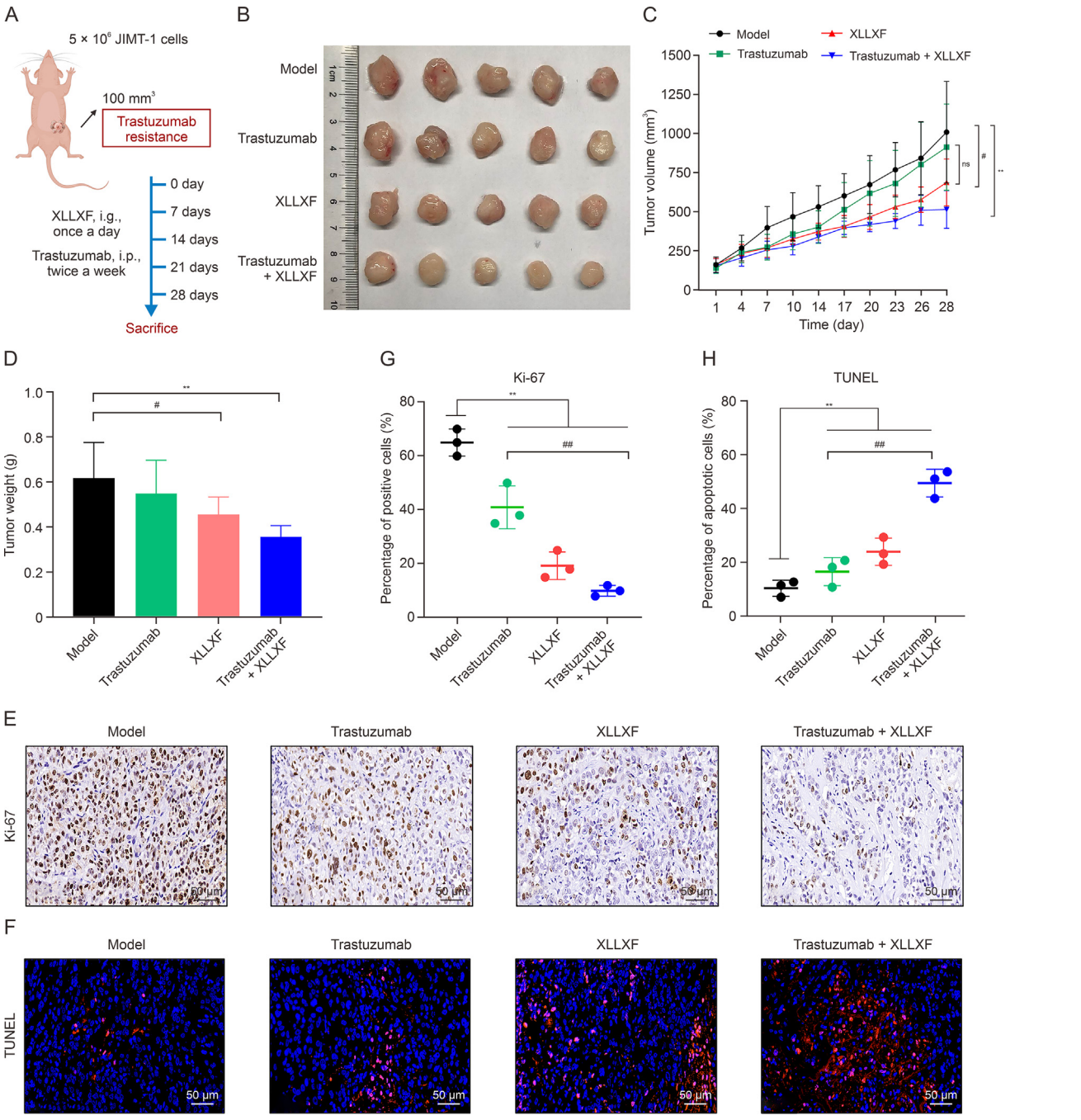

Fig. 2. Xianling Lianxia formula (XLLXF) synergizes with trastuzumab to inhibit the tumor growth in human epidermal growth factor receptor 2 (HER2)-positive breast cancer (BC) bearing mice. (A) Schematic diagram of animal model construction and drug administration by Figdraw. (B) Representative images of tumors with the indicated treatment. (C) Tumor size of each group was measured every three days after treatments started. The tumor size data are plotted and shown as mean ± standard deviation (SD). (D) tumor weight of the dissected tumors at the end point was presented. (E) The proliferative cells in tumor tissues were determined by immunohistochemical staining of Ki-67. (F) The apoptotic cells in tumor tissues of each group were determined by terminal dexynucleotidyl transferase-mediated dUTP nick-end labeling (TUNEL) assay. (G, H) The percentage of proliferative cells (G) and apoptotic cells (H) were quantified using ImageJ. Model group: physiological saline, i.g., once a day; trastuzumab group: trastuzumab, i.p., 5 mg/kg, twice a week; XLLXF group: XLLXF, i.g., 5.26 mg/kg, once a day; trastuzumab + XLLXF group: trastuzumab, i.p., 5 mg/kg, twice a week and XLLXF, i.g., 5.26 mg/kg, once a day. $^{**}P < 0.01$, $^{\#}P < 0.05$, and $^{\#\#}P < 0.01$. ns: not significant.

marker of proliferation, in the tumor tissues of the combination group compared with that of the model control group and the trastuzumab group (Figs. 2E and G). Finally, TUNEL assays showed that the percentage of apoptotic cells significantly increased in the combination group (Figs. 2F and H). These results demonstrated that XLLXF could enhance the antitumor effect of trastuzumab in a resistant mouse model.

3.5. XLLXF increases NK cell activity and function in HER2-positive BC-bearing mice

Similar to NK1.1 in other mouse strains, the marker CD49b was used to label NK cells in BALB/c mice [28]. The combination of XLLXF and trastuzumab boosted the infiltration of NK cells in the tumors (Figs. 3A, 3B, S3A, and S3B). We then examined the functional

receptors and effector particles of NK cells to reflect the function of NK cells. The activity of NK cells undergoes stringent regulation via the balance between inhibitory and activating receptors [29]. NKG2D and NKp46 are major activating receptors [30], whereas NKG2A impedes the anticancer functions of NK cells [31]. Furthermore, non-classical histocompatibility antigen HLA-G acts to desensitize BC cells to trastuzumab by binding to KIR2DL4 [32]. In our study, Western blot analysis demonstrated that the combination of XLLXF with trastuzumab led to a heightened expression of NKG2D and NKp46 and a dampened expression of NKG2A, KIR2DL4, and HLA-G in tumor tissues of HER2-positive BC mice (Figs. 3C and D). NK cells can induce cytotoxicity by releasing perforin and granzyme,

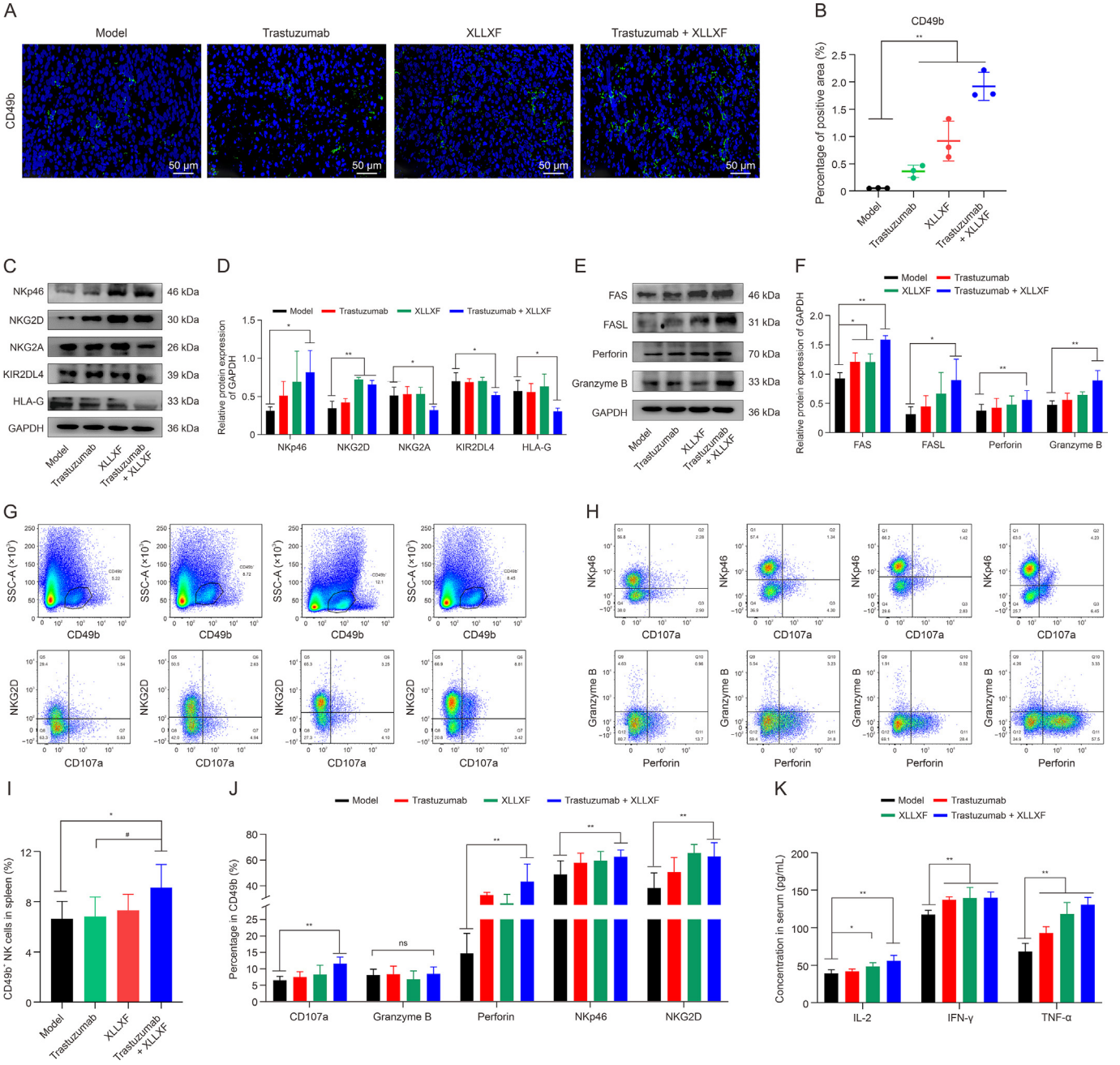

Fig. 3. Xianling Lianxia formula (XLLXF) synergizes trastuzumab to increase natural killer (NK) cell activity and function in human epidermal growth factor receptor 2 (HER2)-positive breast cancer (BC)-bearing mice. (A, B) The infiltration of NK cells in tumor tissues was detected by immunofluorescence staining of CD49b (A), and the percentage was quantified using ImageJ (B). Similar to NK1.1 in other mouse strains, the marker CD49b was used to label NK cells in BALB/c mice. (C, D) The protein expressions of NKp46, NK group 2 member D (NKG2D), NK group 2 member A (NKG2A), killer cell immunoglobulin-like receptor 2DL4 (KIR2DL4), and human leucocyte antigen-G (HLA-G) were performed by Western blot (C), and quantified analysis was performed by ImageJ (D). (E, F) The protein expressions of factor-associated suicide (FAS), factor-associated suicide ligand (FASL), perforin, and granzyme B in mouse tumor tissues from different treatment groups were performed by Western blot (E), and quantified analysis was performed by ImageJ (F). Data presented as mean ± standard deviation (SD) normalized to glyceraldehyde-3-phosphate dehydrogenase (GAPDH) levels. (G–H) NK cells ($CD49b^+$ populations) isolated from the spleens of tumor-bearing mice and NKG2D (G) and NKp46, CD107a, granzyme B, and perforin (H) in the NK cells were analyzed by flow cytometry. (I, J) Statistical analysis of the percentages of $CD49b^+$ NK cells in spleen (I), and CD107a, granzyme B, perforin, NKp46, and NKG2D (J). (K) The serum interleukin (IL)-2, interferon-gamma (IFN-γ), and tumor necrosis factor-alpha (TNF-α) levels were quantified by enzyme-linked immunosorbent assay (ELISA). Data are presented as mean ± standard deviation (SD). Model group: physiological saline, i.g., once a day; trastuzumab group: trastuzumab, i.p., 5 mg/kg, twice a week; XLLXF group: XLLXF, i.g., 5.26 mg/kg, once a day; trastuzumab + XLLXF group: trastuzumab, i.p., 5 mg/kg, twice a week and XLLXF, i.g., 5.26 mg/kg, once a day. $^{*}P < 0.05$, $^{**}P < 0.01$, and $^{\#}P < 0.05$. SSC-A: side scatter-area.

expressing FASL, and secreting cytokines [33]. We found that the combination group exhibited high positive rates of perforin and granzyme B compared with the model group (Figs. 3E, 3F, S3C, and S3D). In tumor tissues, we observed a statistically significant increase in the expression of FAS and FASL following treatment with the combination (Figs. 3E, 3F, S3E, and S3F).

Concurrently, we investigated the percentage of NK cells, their activating receptors, and cytotoxic granules in the spleen by flow cytometry. Through the gating method provided in Fig. S1, we found that the combination of XLLXF and trastuzumab increased the number of $CD49b^+$ NK cells in the spleen, as well as the expressions of CD107a, perforin, NKp46, and NKG2D (Figs. 3G–J). However, there was no statistically significant difference in granzyme B expression between the four groups. The activity of NK cells was also evaluated by measuring the serum levels of IL-2, TNF-α, and IFN-γ, which increased following the treatments of XLLXF, trastuzumab, or their combination; they increased most in the combination group (Fig. 3K). These results revealed that the synergistic effects of XLLXF on trastuzumab might be associated with the improvement of NK cells.

3.6. Depletion of NK cells attenuates the potentiating effect of XLLXF on trastuzumab in HER2-positive BC-bearing mice

Furthermore, we attempted to confirm the importance of NK cells in the synergistic antitumor effects of XLLXF and trastuzumab on HER2-positive BC. Anti-ASGM-1 antibody, which can deplete NK cells, its isotype IgG, and other treatments were given to the tumor-bearing mice at the indicated time intervals (Fig. 4A). The potentiating impact of XLLXF on the efficacy of trastuzumab was attenuated following the reduction of NK cells (Figs. 4B–D). Flow cytometry showed that NK cells had been successfully depleted by regular interventions of anti-ASGM-1 antibodies (Figs. 4E and F). Compared with anti-ASGM-1 antibody, the addition of IgG isotype control maintained the pronounced proliferation inhibitory and pro-apoptotic effects on tumor tissues by XLLXF combined with trastuzumab (Figs. 4G–I). Thus, NK cells played a critical role in the synergized treatment of XLLXF combined with trastuzumab in HER2-positive BC.

3.7. XLLXF synergizes trastuzumab to enhance the ADCC effect

NK cell-mediated ADCC has a significant impact on its therapeutic efficacy in anti-HER2-targeted treatment. To address whether XLLXF can improve the tumor-killing capacity of NK cells and the ADCC effect mediated by them, we used a co-culture system of human NK cells together with HER2-positive BC cells. At day 14 of expansion, human peripheral blood mononuclear cells (PBMCs) attained peak purity (86.16% $CD3^-CD56^+$ cells) and maturity (95.64% $CD3^-CD56^+CD16^+$ cells) of NK cells (Figs. 5A and B), rendering them suitable for use as effector cells in subsequent experiments. NK cells were pre-treated with 100 μg/mL XLLXF (XLLXF-NK) or vehicle control (NK) for 48 h before being subjected to co-culture with CFSE-labeled SK-BR-3 and JIMT-1 cells under different E:T ratios (Fig. 5C). In this co-culture system, the expression of NKp46 in NK cells with or without trastuzumab was significantly increased by XLLXF pre-treatment, except that at the E:T ratio of 5:1 when trastuzumab was administered to the co-culture system (Figs. 5D and E).

In the absence of trastuzumab, XLLXF intervention enhanced the cytosiss ability of NK cells in co-cultures with SK-BR-3 cells at an E:T ratio of 10:1, as well as with JIMT-1 cells at E:T ratios of 5:1 and 10:1 (Figs. 5F and G; green vs. black). We used a concentration of 2.7 μM trastuzumab to induce the ADCC effect of NK cells (red vs. black). The ADCC effect was significantly enhanced by the pre-treatment of NK cells with XLLXF, in co-cultures with SK-BR-3 cells at E:T ratios of 5:1 and 10:1, as well as with JIMT-1 cells at E:T ratios of 3:1 and 5:1 (Figs. 5F and G, blue vs. red).

IL-15 is known to play a crucial role in the proliferation and activation of NK cells [34]. Our findings indicated that, in the presence of trastuzumab, XLLXF significantly enhanced the production of IL-15 and IFN-γ (Figs. 5H and I). Additionally, Western blot analysis of the NK cells revealed that NKG2D, NKp46, perforin, and granzyme B were modulated by different treatments. Specifically, the combination of trastuzumab and XLLXF enhanced the protein expression of NKG2D, NKp46, perforin, and granzyme B in the co-cultured NK cells (Figs. 5J–L).

3.8. XLLXF pre-treatment on NK cells significantly increases their tumor-killing capacity

To comprehensively evaluate the impact of XLLXF on the antitumor activity of human NK cells, we conducted an intervention study involving adoptive cellular immunotherapy (ACT). Specifically, NK cells pre-treated with either control or XLLXF were injected at multiple time points into tumor-bearing nude mice, with or without trastuzumab treatment (Fig. 6A). Trastuzumab treatment did not curb the development of these drug-resistant tumors in nude mice. However, when trastuzumab treatment was combined with NK cells pretreated with XLLXF, we observed a significant reduction in tumor growth compared with either no-treatment control or the combination of trastuzumab and NK cells pretreated with vehicle (Figs. 6B–D). The biocompatibility of XLLXF-NK cells was also evaluated by monitoring the body weight of host mice, and no significant body weight loss was observed across all tested experimental groups (Fig. 6E). Notably, trastuzumab single treatment did not change the proliferation rate of the tumor compared with the model control group. NK cell injection reduced tumor proliferation, whereas the trastuzumab combined with XLLXF-NK cell treatment group exhibited the strongest inhibition on tumor proliferation (Figs. 6F and G). Furthermore, we observed that XLLXF-NK cells combined with trastuzumab treatment had the greatest NK cell infiltration into the tumor (Figs. 6H and I). Taken together, the results showed that XLLXF pre-treatment on NK cells significantly increased the tumor-killing capacity in the presence of trastuzumab.

3.9. RNA-seq revealed the targets and signaling pathways of NK cells regulated by XLLXF

To investigate the effects of XLLXF on NK cell gene expression and signaling pathways, we conducted RNA-seq analysis on NK cells isolated from the spleens of tumor-bearing mice and compared those treated with XLLXF with those without any treatment. Consistent with previous studies, XLLXF possesses the ability to significantly curb the proliferation of tumors in a four-week dosage (Figs. 7A–C). NK cells from the spleens were purified through magnetic bead separation (Fig. 7D). XLLXF provoked the downregulation of 501 genes and upregulation of 480 genes within the NK cells (FC > 1.2 and $P < 0.05$; Figs. 7E and F). KEGG enrichment analysis indicated that the significantly enriched signaling pathways included NK cell-mediated cytotoxicity, Janus-activated kinase/signal transducer and activator of transcription (JAK/STAT) signaling pathway, cytokine-receptor interaction, and chemokine signaling pathway (Fig. 7G).

Among the upregulated genes, a considerable proportion was observed to be closely linked with NK cell activity, such as *CISH* (log2FC = −1.01, $P < 0.001$), *NKp46* (log2FC = 1.33, $P < 0.001$), *NKG2D* (log2FC = 0.92, $P < 0.001$), *perforin* (log2FC = 1.44,

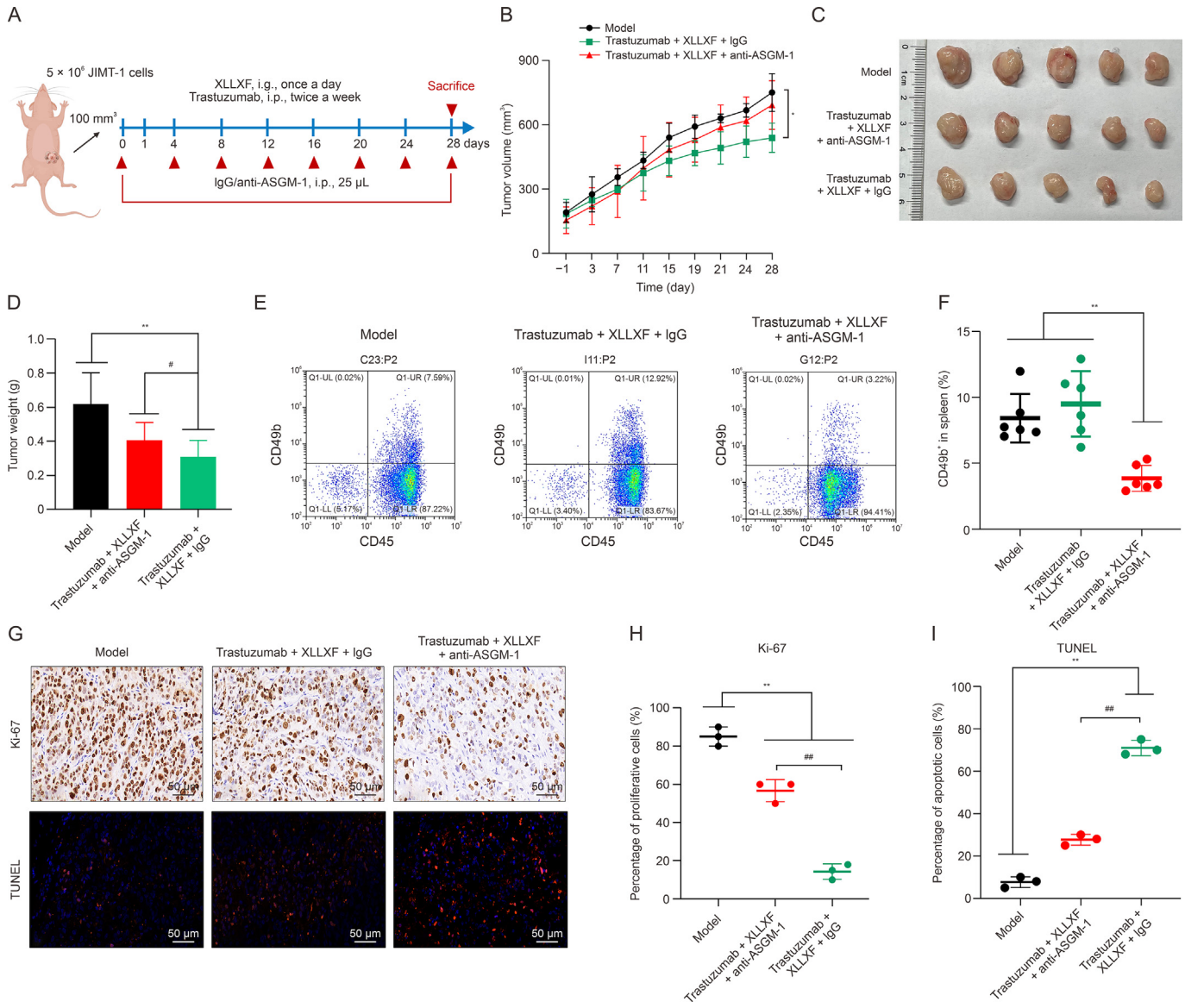

Fig. 4. Depletion of natural killer (NK) cells attenuates the potentiating effect of Xianling Lianxia formula (XLLXF) on trastuzumab in human epidermal growth factor receptor 2 (HER2)-positive breast cancer (BC)-bearing mice. (A) Schematic diagram of the model construction and intervention process by Figdraw. (B) Tumor size of each group was measured after treatments started. The tumor size data are plotted and shown as mean ± standard deviation (SD). (C) Representative images of tumors with the indicated treatment. (D) Tumor weight of the dissected tumors at the end point was presented. (E, F) The flow charts (E) and percentages (F) of NK cells ($CD49b^+$ populations) isolated from the spleens of tumor-bearing mice after continuously interventions for four weeks were performed by flow cytometry. (G) The proliferative and apoptotic cells in tumor tissues were determined by immunohistochemical staining of Ki-67 and dexynucleotidyl transferase-mediated dUTP nick end labeling (TUNEL). (H, I) The percentages of proliferative cells (H) and apoptotic cells (I) were quantified using ImageJ. Model group: physiological saline, i.g., once a day; trastuzumab + XLLXF + IgG group: trastuzumab, i.p., 5 mg/kg, twice a day, XLLXF, i.g., 5.26 mg/kg, once a day, and IgG, i.p., 15 mg/kg, every three days; and trastuzumab + XLLXF + anti-asialo GM-1 (anti-ASGM-1) group: trastuzumab, i.p., 5 mg/kg, twice a day, XLLXF, i.g., 5.26 mg/kg, once a day, and anti-ASGM1, i.p., 25 μL, every three days. $^{*}P < 0.05$, $^{**}P < 0.01$, $^{\#}P < 0.05$, and $^{\#\#}P < 0.01$. UL: upper left; UR: upper right; LR: lower right; LL: lower left.

$P < 0.001$), *FASL* (log2FC = 1.49, $P < 0.001$), and X–C motif chemokine ligand 1 (*XCL1*) (log2FC = 1.62, $P < 0.001$) (Fig. 7H).

CISH, identified as a key inhibitor of cytokine signaling, impedes the ability of IL-15 to stimulate NK cells primarily through the JAK/STAT pathway [35]. Even at low concentration levels of IL-15, suppression of *CISH* improves the activation and functionality of NK cells [36]. Our RNA-seq results revealed that XLLXF led to a significant reduction in *CISH* expression with a FC of 2.01 ($P < 0.001$; Fig. 7I).

To verify whether XLLXF regulates NK cells by suppressing *CISH* and increasing JAK/STAT signaling, we isolated the spleen NK cells from tumor-bearing mice after four consecutive weeks of XLLXF intervention to analyze their protein levels. NKp46 and NKG2D were significantly upregulated, whereas the protein expression of CISH was notably downregulated (Fig. 7J). The impact of XLLXF on primary human NK cells was also analyzed in the *in vitro* culture and demonstrated similar effects on these proteins (Fig. 7J). Furthermore, XLLXF exhibited a significant enhancement in the levels of p-JAK1 and p-STAT5 in the human NK cells without changing JAK1 and STAT5 protein levels (Fig. 7K). In conclusion, XLLXF significantly regulates CISH, NKp46, NKG2D, and JAK/STAT pathway in both spleen NK cells and primary human NK cells (Figs. 7L–N).

3.10. XLLXF enhances NK cell activity and ADCC effect by inhibiting CISH expression and enhancing JAK1/STAT5 signaling

To validate the importance of *CISH* in the modulation of NK cells by XLLXF, we silenced the *CISH* gene in human primary NK cells via

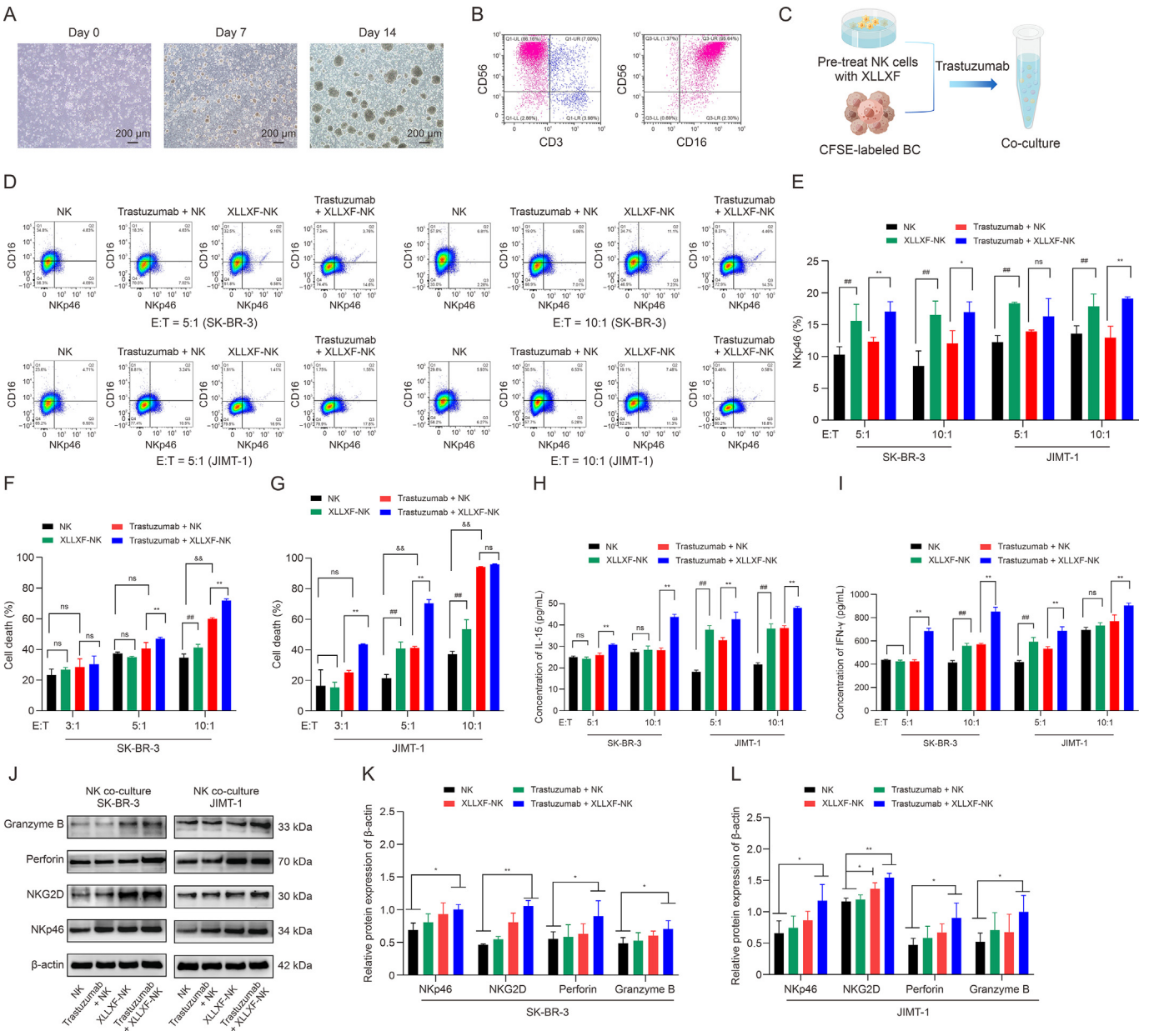

Fig. 5. Xianling Lianxia formula (XLLXF) synergizes trastuzumab to enhance the antibody-dependent cell cytotoxicity effect. (A) The expansion of human peripheral blood mononuclear cell (PBMC)-derived primary natural killer (NK) cells *in vitro*. From left to right, PBMCs were cultured for day 0, 7, and 14. (B) Flow cytometry analysis of the human PBMC-derived primary NK cells ($CD3^{-}CD56^{+}CD16^{+}$ cells). (C) Schematic diagram of the construction of the co-culture system of NK cells and breast cancer (BC) cells. NK cells pretreated with XLLXF or vehicle control were subjected to co-culture with carboxyfluorescein succinimidyl ester (CFSE)-labeled SK-BR-3 and JIMT-1 cells under the indicated ratios of effector (NK cells)-to-target (SK-BR-3/JIMT-1 cells). (D, E) The flow charts (D) and percentages (F) of $NKp46^{+}$ in NK cells from different treatment groups were performed by flow cytometry. (F, G) Cytotoxicity was quantified by calculating the percentage of allophycocyanin (APC)-positive cells in all target cells by flow cytometry analysis: CFSE-labeled SK-BR-3 (F) and JIMT-1 cells (G) were stained for dead cells with APC-live/dead fixable aqua dead cell stain kit for 30 min on ice. (H, I) The interleukin (IL)-15 (H) and interferon-gamma (IFN-γ) (I) levels in the co-cultured supernatant were quantified by enzyme-linked immunosorbent assay (ELISA). (J–L) The protein expressions of granzyme B, perforin, NK group 2 member D (NKG2D), and NKp46 (J) in NK cells after co-culturing with SK-BR-3 cells (K) or JIMT-1 cells (L) were performed by Western blot. All band intensities were quantified by ImageJ and data presented as mean ± standard deviation (SD) normalized to glyceraldehyde-3-phosphate dehydrogenase (GAPDH) levels. NK group: NK cells co-cultured with breast cancer; XLLXF-NK group: NK cells co-cultured with breast cancer cells after 24 h of XLLXF pre-treatment; trastuzumab + NK group: trastuzumab added at the same time as NK cells co-cultured with breast cancer; and trastuzumab + XLLXF + NK group: trastuzumab added at the same time as NK cells co-cultured with breast cancer cells after XLLXF pre-treatment for 24 h. $^{*}P < 0.05$, $^{**}P < 0.01$, $^{\#\#}P < 0.01$, and $^{\&\&}P < 0.01$; ns: not significant. UL: upper left; UR: upper right; LR: lower right; LL: lower left; E:T: effector-to-target.

siRNA transfection. After transfection with No. 2 siRNA-*CISH*, the protein and gene expression levels of *CISH* were significantly inhibited in human primary NK cells analyzed by Western blot and RT-PCR, respectively (Figs. 8A, 8B, and S4 and Table S6).

Subsequently, we established a co-culture system of NK cells with JIMT-1 cells consistent with the previous method (Fig. 5C). Flow cytometry analysis demonstrated that NK cells expressing lower levels of *CISH* exhibited a significantly enhanced ADCC effect compared with the negative control siRNA (NC) control group (Fig. 8C). The cell viability of JIMT-1 cells was notably inhibited by *CISH*-low NK cells at different E:T ratios (Fig. 8D). Notably, even though the intervention of XLLXF raised the levels of NKp46, p-JAK1, and p-STAT5, we found no significant differences in the BC inhibitory effect of *CISH*-low NK cells pretreated with XLLXF (Figs.

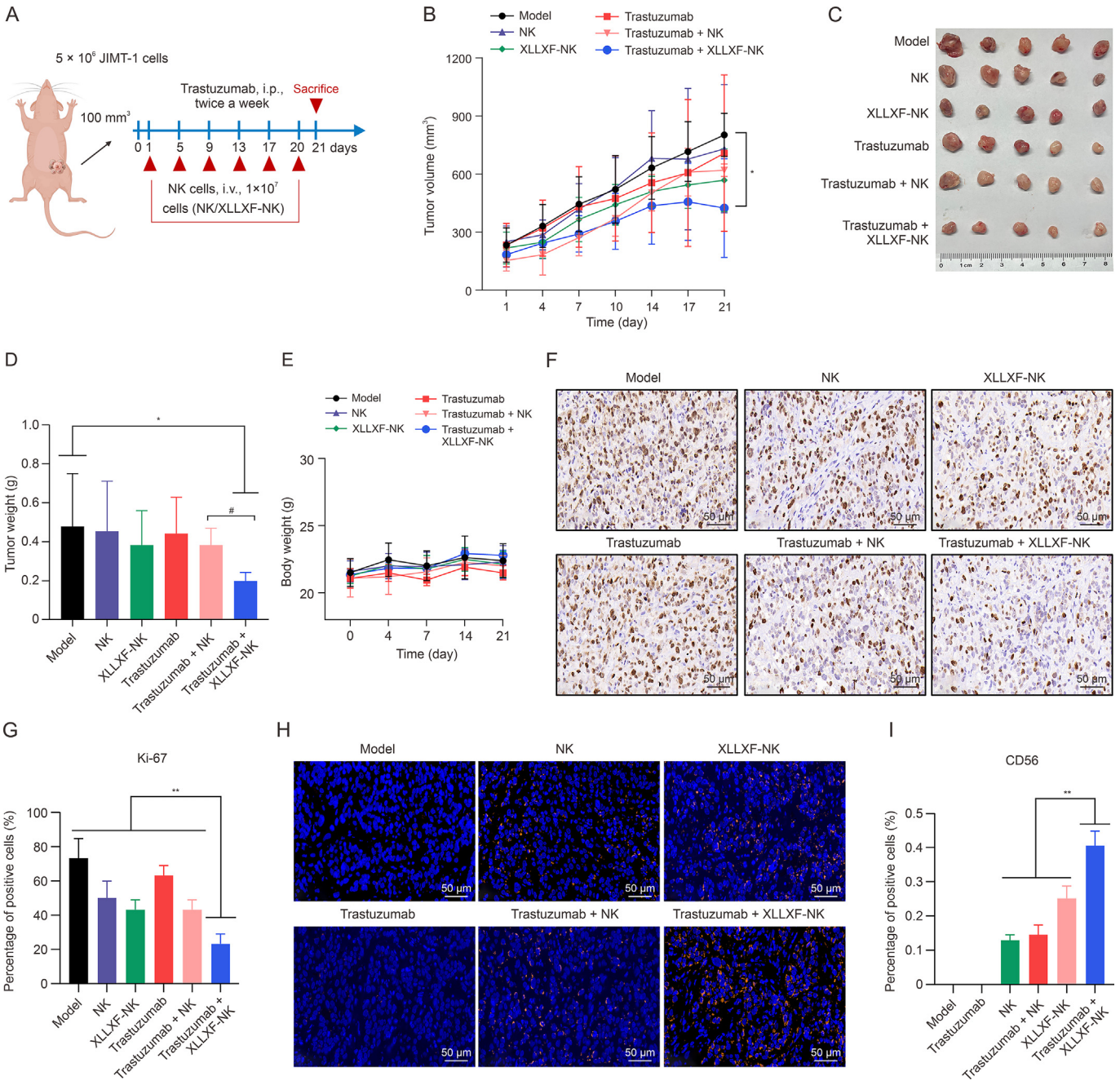

Fig. 6. Xianling Lianxia formula (XLLXF) pre-treatment on natural killer (NK) cells significantly increases their tumor-killing capacity. (A) Schematic diagram of the model construction and intervention process by Figdraw. (B) Tumor size of each group was measured after treatments started. The tumor size data are plotted and shown as mean ± standard deviation (SD). (C) Representative images of tumors with the indicated treatment. (D) Tumor weight of the dissected tumors at the end point was presented. (E) Statistical diagram of body weight of the nude mice with indicated treatment. (F, G) The percentage of proliferative cells in tumor tissues was determined by the immunohistochemical staining of Ki-67 (F), and the percentage was quantified using ImageJ (G). (H, I) The percentage of NK cells in tumor tissues was determined by the immunofluorescent staining of CD56 (H), and the percentage was quantified using ImageJ (I) ($n = 5$). Model group: physiological saline, i.v., twice a week; NK group: 1×10^7 NK cells, i.v., twice a week; XLLXF-NK group: 1×10^7 NK cells pretreated with 100 μg/mL XLLXF for 48 h, i.v., twice a week; trastuzumab group: trastuzumab, i.p., 5 mg/kg, twice a week; trastuzumab + NK group: trastuzumab, i.p., 5 mg/kg, twice a week, and 1×10^7 NK cells, i.v., twice a week; and trastuzumab + XLLXF-NK group: trastuzumab, i.p., 5 mg/kg, twice a week, and 1×10^7 NK cells pretreated with 100 μg/mL XLLXF for 48 h, i.v., twice a week. $^{*}P < 0.05$, $^{**}P < 0.01$, and $^{\#}P < 0.05$.

8C and D). High expression of NKp46 in *CISH*-low NK cells was observed (Figs. 8E and F). Additionally, the protein expression of NKp46 and NKG2D and the phosphorylation of JAK1 and STAT5 were observed to be significantly enhanced when *CISH* was knocked down, regardless of XLLXF pretreatment (Figs. 8G–J). This result may be because XLLXF has multiple activation pathways for JAK1/STAT5 signaling, but its enhancement of NK cell function is mainly mediated by *CISH*. In conclusion, these findings suggested that XLLXF could enhance the activity of NK cells and the ADCC effect by promoting JAK1/STAT5 signaling and limiting *CISH* expression.

3.11. Potential active ingredients of XLLXF

The chemical constituents of XLLXF were analyzed by UPLC-QE-MS/MS. Our findings revealed a total of 528 chemical components

that belong to various classes, including flavonoids, amino acids, peptides and derivatives, terpenes, fatty acyls, phenylpropanoids, carbohydrates and glycosides, organic acids and derivatives, nucleotides and derivatives, alkaloids, glycerophospholipids, phenols, pyridines and derivatives, indoles and derivatives, glycerolipids, imidazopyrimidines, pteridines and derivatives, and others. The total ion chromatogram (TIC) of the samples is displayed in Fig. S5. A total of 45 compounds with prototype structures, such as flavones, flavonols, glycosides, and isoflavones, were identified in the plasma samples of the mice that were administered with XLLXF (Table S7).

3.12. Effect of active ingredients in XLLXF on NK cells

Further investigations were conducted to elucidate the influence of active ingredients in XLLXF on NK cells. On the basis of UPLC-QE-MS analysis, we selected icariin from XLP, lobetyolin from DS, curcumenol from EZ, and scutellarein from BZL as the main components. The results indicated that scutellarein and lobetyolin significantly enhanced NK cell proliferation in a dose-dependent manner (Figs. 9A–D). Icariin exerted a significant proliferative effect on NK cells at a concentration of 64 μM (Figs. 9E and F), whereas curcumenol did not significantly affect NK cell proliferation (Figs. 9G and H). Subsequently, the intervention concentrations of 0, 4, 16, and 64 μM were selected to examine the effects of the four active components on NKp46 via flow cytometry. The results revealed that all four components increased the proportion of NKp46 in $CD3^{-}CD56^{+}$ cells after 24 h of intervention at different concentrations, with the most pronounced effect observed at 64 μM (Figs. 9I–L). These intriguing findings provide valuable insights for our subsequent screening of active components that can enhance NK cell activity.

4. Discussion

As the first HER2-targeted therapy approved by the U.S. Food and Drug Administration, trastuzumab selectively exerts antitumor effects in patients with HER2-positive BC [37]. Trastuzumab is a humanized recombinant monoclonal antibody to HER2 and binds to HER2 domain IV, close to the HER2 juxta-membrane region. Many mechanisms have been proposed for the antitumor activity of trastuzumab, including inhibiting HER2 heterodimer activation, promoting NK cell-mediated ADCC effect, blocking intracellular tyrosine kinase activation, inhibiting tumor cell proliferation and survival, inhibiting signaling pathways such as mammalian target of rapamycin (mTOR), mitogen-activated protein kinase (MAPK), and phosphatidylinositol 3-kinase (PI3K), inhibiting DNA damage repair, and suppressing angiogenesis [38,39].

However, failure with trastuzumab occurs, and most patients who are insensitive to trastuzumab do not achieve long-term benefits when switched to other HER2-targeted drugs [40]. Research suggested that the tumor immune microenvironment is a crucial factor in determining prognosis. Shang et al. [41] conducted a multifactor logistic regression analysis on 155 HER2-positive BC cases undergoing neoadjuvant therapy. Their study found that elevated levels of tumor-infiltrating lymphocytes are independent predictors of achieving a complete pathological response (pCR) during treatment [41]. An increasing amount of research suggested that the success of trastuzumab in treating HER2-positive BC depends on the innate immune response, including NK cell-mediated ADCC and macrophage-mediated antibody-dependent cell phagocytosis [42,43]. Our study found that XLLXF could enhance the activity of NK cells in patients with HER2-positive BC. Further investigations confirmed that the combination of XLLXF and trastuzumab effectively inhibited the growth of HER2-positive BC tumors in mice. The inhibitory effect of XLLXF was weakened when NK cells were depleted. Notably, XLLXF significantly improved the ADCC effect and cytotoxicity of human NK cells compared with mice. These research findings increase our confidence in the potential therapeutic use of XLLXF in treating patients.

BALB/c nude mice were used in our experiment to construct the animal model due to the human origin HER2-positive BC cell lines. The nude mice are homozygous for a mutation in the forkhead box N1 (*Foxn1*) gene, which causes hairlessness and impaired development of the thymus, resulting in an inability to generate mature T cells [44]. Despite having a low number of peripheral T cells, they have intact innate immune function, especially high activity of NK cells [45]. Although the model has certain disadvantages, it is still considered as an indispensable tool in many fields of cancer research, particularly in the discovery of new drugs that can effectively combat cancer or enhance the efficacy of current chemotherapy [46,47].

CISH, a member of the suppressor of the cytokine signaling family, exerts inhibitory effects on JAK/STAT signaling in NK cells [48]. RNA-seq revealed that XLLXF downregulated the expression of the *CISH* gene by 2.1 fold, showing a statistically significant difference compared with model controls ($P < 0.001$). Zhu et al. [36] suggested that IL-15-mediated JAK/STAT signaling activity is enhanced in $CISH^{-/-}$iPSC-NK cells, leading to increased cytotoxic activity, even at low IL-15 concentrations. Additionally, TGF-β has suppressive effects on immunity in the tumor microenvironment, which impairs the function of NK cells. Nevertheless, when *TGF-β* and *CISH* were simultaneously depleted in NK cells, antitumor immunity was considerably enhanced [49]. Bi et al. [50] demonstrated that the combination of TNF-α-induced protein-8 like-2 (*TIPE2*) and *CISH* deficiency can enhance the antitumor activity of NK cells [50]. We found that *CISH*-low NK cells exhibited high levels of NKp46 and NKG2D expression, high JAK1 and STAT5 phosphorylation, and strong ADCC effects. Interestingly, the synergistic antitumor effect of trastuzumab and XLLXF with *CISH*-low NK cells was relatively limited, suggesting that suppressing *CISH* expression is an essential way, by which XLLXF enhances the NK cell-mediated ADCC effect.

Currently, clinical trials are evaluating chimeric antigen receptor (CAR)-based ACT using CAR-T and CAR-NK cells for both hematological and solid tumors [51,52]. Compared with CAR-T cells, NK cells are less likely to induce severe graft-versus-host disease, neurotoxicity, or cytokine release syndrome [53]. As a result, NK cells have shown superior effectiveness and safety in the treatment of solid tumors [54,55].

However, limitations of CAR-NK efficacy need to be addressed. First, CAR-NK cells have low *in vivo* activation and persistence after being transplanted back into patients. Therefore, *ex vivo* expansion before reinfusion is required to prepare a good quantity of cells able to infiltrate into tumors [56,57]. While it may be safe, this limitation can restrict the efficacy of NK cell immunotherapy. Efforts are being made to transduce NK cells with constructs to express cytokines or modify other related genes. However, safety is one issue, and the low transduction rate of NK cells is another [58,59]. In our research, XLLXF was found to increase the expression of cytokines, such as IL2 and IFN-γ, and inhibit the expression of *CISH*. These findings suggested that NK cells treated with XLLXF may require less preprocessing involving cytokine reduction and gene editing, thereby reducing the aforementioned risks. Moreover, NK cells exhibited strong persistence and activation in patients with HER2-positive BC and mice receiving long-term treatment with XLLXF. Rapid homing to tumor tissue is crucial for the effectiveness of NK cell adoptive therapy [60,61]. The intricate interplay between chemokines released by NK cells and tumor cells regulates this process, and efforts are being made to improve the efficiency of homing to tumor tissues. In this study, in mouse-derived NK cells and in human NK

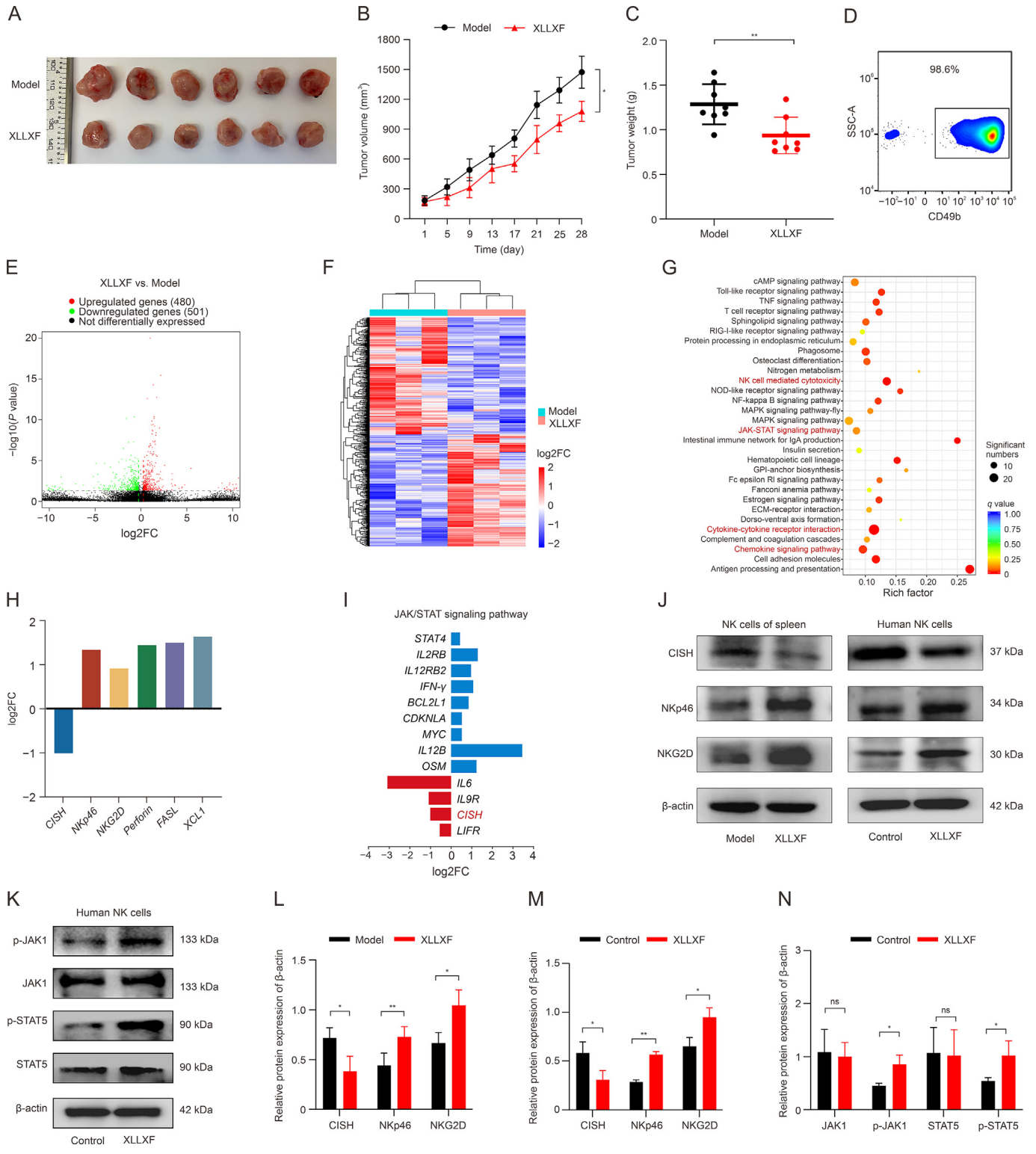

Fig. 7. RNA sequencing (RNA-seq) revealed the targets and signaling pathways of natural killer (NK) cells regulated by Xianling Lianxia formula (XLLXF). (A) Representative images of tumors from JIMT-1 xenografted mice with the indicated treatment. (B) Tumor size of each group was measured after treatments started. The tumor size data are plotted and shown as mean ± standard deviation (SD) ($n = 6$). (C) Tumor weight of the dissected tumors at the end point was presented. (D) NK cells of the spleen were purified by negative magnetic selection using an NK Cell Isolation Kit. The purity of isolated NK cells ($CD49b^+$ populations) was determined by flow cytometry analysis. (E–G) Volcano plot (E), heatmap (F), and Kyoto Encyclopedia of Genes and Genomes (KEGG) enrichment analysis (G) of differentially expressed genes (DEGs) in spleen-derived NK cells from the model and XLLXF groups. (H) A bar graph showing key genes regulated by XLLXF, which are associated with NK cell function. (I) A bar graph showing Janus kinase 1 (JAK1)/signal transducer and activator of transcription 5 (STAT5) signaling pathway key genes differentially expressed in the two groups. Among them, cytokine inducible Src homology 2 (SH2) containing protein (*CISH*) was highlighted. (J–N) The protein expressions of CISH, NKp46, and NK group 2 member D (NKG2D) in the spleen NK cells and human NK cells (J), and p-JAK1, JAK1, STAT5, and p-STAT5 in human NK cells (K) from different treatment groups were performed by Western blot. Quantified analyses of CISH, NKp46, and NKG2D in the spleen NK cells (L) and human NK cells (M), and JAK1, p-JAK1, STAT5, and p-STAT5 in human NK cells (N) were performed by ImageJ. Data presented as mean ± standard deviation (SD) normalized to β-actin levels. Model group: physiological saline, i.g., once a day; XLLXF: XLLXF, i.g., 5.26 mg/kg, once a day. $^*P < 0.05$ and $^{**}P < 0.01$; ns: not significant. SSC-A: side scatter-area;

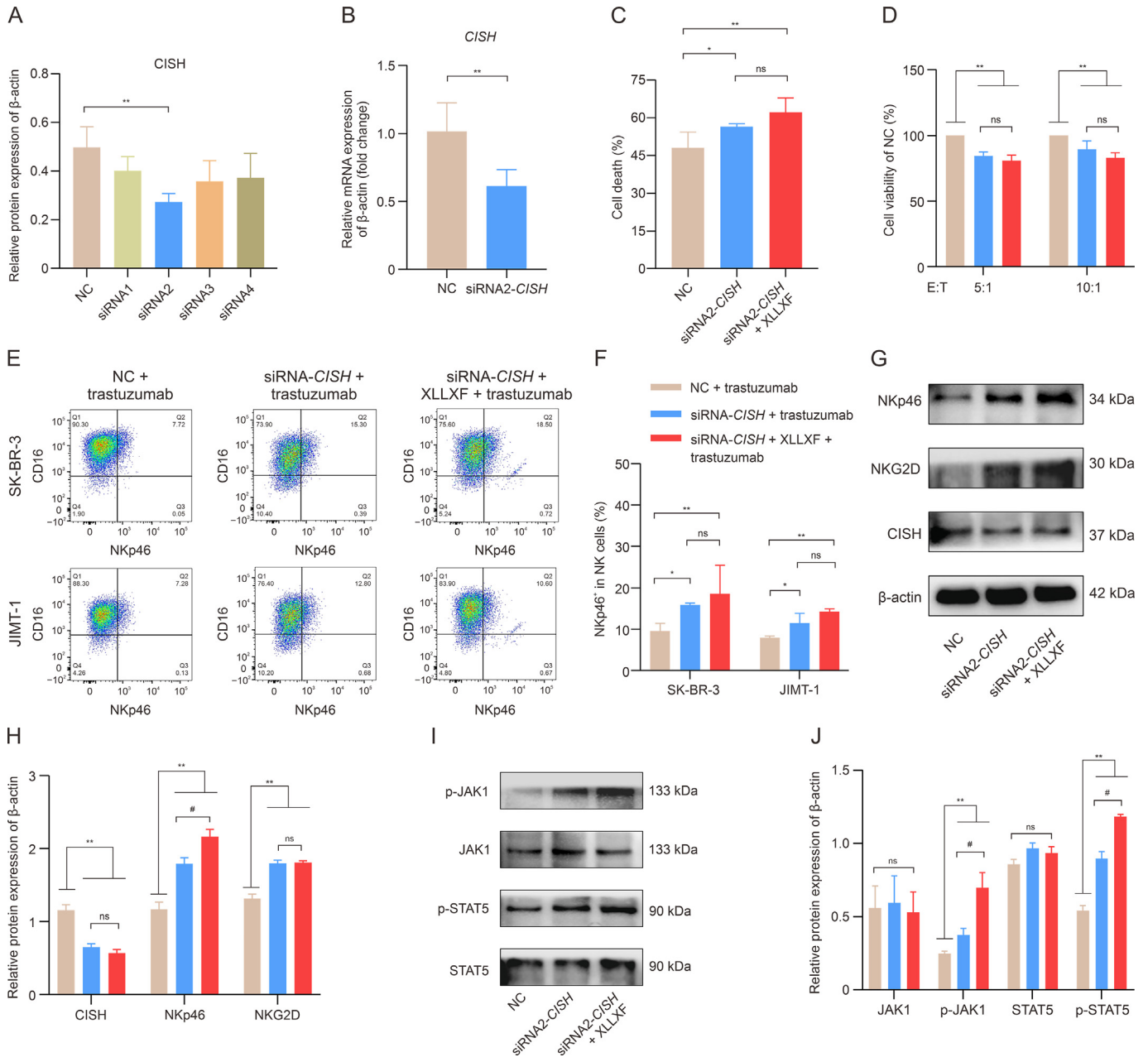

Fig. 8. Xianling Lianxia formula (XLLXF) enhances natural killer (NK) cell activity and antibody-dependent cell cytotoxicity effect by inhibiting cytokine inducible Src homology 2 (SH2) containing protein (*CISH*) expression and enhancing Janus kinase 1 (JAK1)/signal transducer and activator of transcription 5 (STAT5) signaling. (A, B) Protein (A) and messenger RNA (mRNA) (B) levels of *CISH* in NK cells by Western blot analysis and reverse transcription-polymerase chain reaction (RT-PCR), respectively. The cells were collected 72 and 48 h after transfection, respectively. (C) The normal control (NC) and small interfering RNA (siRNA)-*CISH* (knockdown) transfected NK cells pretreated with XLLXF or vehicle control were subjected to co-culture with carboxyfluorescein succinimidyl ester (CFSE)-labeled human epidermal growth factor receptor 2 (HER2)-positive breast cancer (BC) JIMT-1 cells, at the presence of trastuzumab (2.7 μM). After 4 h, cytotoxicity was quantified by calculating the percentage of dead cells in all target cells by flow cytometry analysis. (D) In the effector-to-target cells (E:T) ratios of 5:1 and 10:1, cell viability of JIMT-1 cells was determined by Cell Counting Kit-8 (CCK-8) assay after 24 h and data presented as mean ± standard deviation (SD) normalized to NC. (E, F) Flow cytometry analysis (E) was performed to determine the percentage of $NKp46^+$ in NK cells (F) from the same co-culture system with both JIMT-1 and SK-BR-3 cells at an E:T ratio of 3:1, at the presence of trastuzumab. (G, H) The protein expressions of NKp46, NK group 2 member D (NKG2D), and CISH (G) extracted from NK cells after 24 h co-culturing were performed by Western blot, and quantified analysis was performed by ImageJ (H). (I, J) The protein expressions of p-JAK1, JAK1, p-STAT5, and STAT5 were performed by Western blot (I), and the quantified analysis was performed by ImageJ (J). Data presented as mean ± (SD) normalized to β-actin levels. $^{*}P < 0.05$, $^{**}P < 0.01$, and $^{\#}P < 0.05$. ns: not significant.

cells, treatment with XLLXF increased the infiltration of NK cells into the tumor, suggesting that XLLXF could be an effective approach to improve the efficiency of NK cells homing to tumor tissues.

For centuries, TCM has been an alternative therapy utilized in the treatment of a wide range of human diseases. On the basis of several thousand years of herbal medicine experience, herbs were

FC: fold change; cAMP: cyclic adenosine monophosphate; TNF: tumor necrosis factor; RIG-I: retinoic acid-inducible gene I; NOD: nucleotide-binding oligomerization domain; MAPK: mitogen-activated protein kinase; GPI: glycosylphosphatidylinositol; RI: receptor I; ECM: extracellular matrix; FASL: factor-associated suicide ligand; *XCL1*: X–C motif chemokine ligand 1; IL2RB: interleukin (IL)-2 receptor subunit beta; IFN: interferon; BCL2L1: B-cell Llymphoma-2 like protein 1; CDKNLA: cyclin-dependent kinase inhibitor 1A; MYC: myelocytomatosis viral oncogene homolog; OSM: oncostatin M; LIFR: leukemia inhibitory factor receptor; JAK: Janus kinase.

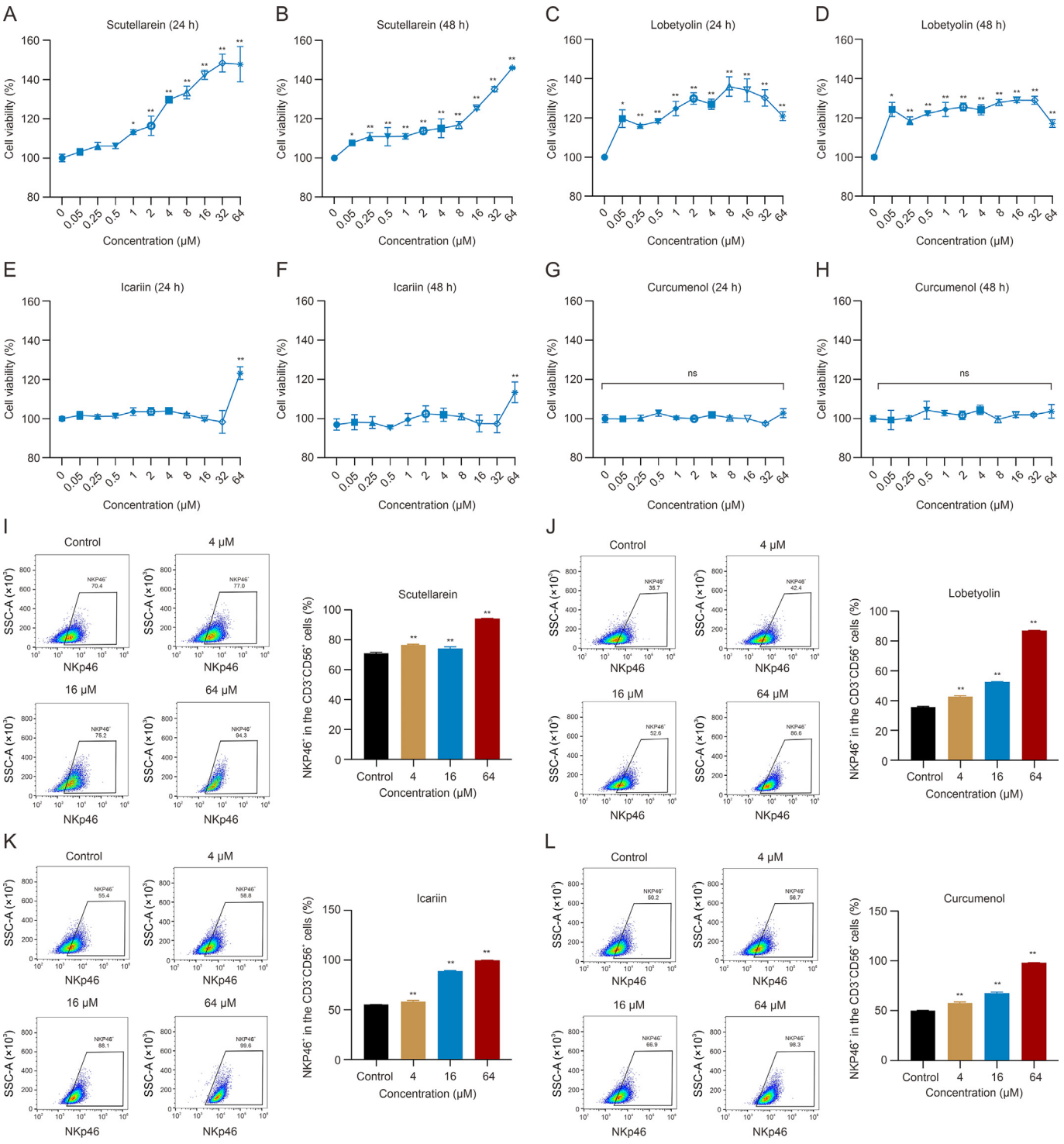

Fig. 9. Effect of active ingredients in Xianling Lianxia formula (XLLXF) on natural killer (NK) cells. (A–H) Potential active ingredients of XLLXF on NK cells: at the indicated concentrations, the effect of scutellarein after intervening for 24 h (A) and 48 h (B), the effect of lobetyolin after intervening for 24 h (C) and 48 h (D), the effect of icariin after intervening for 24 h (E) and 48 h (F), and the effect of curcumenol after intervening for 24 h (G) and 48 h (H) on the proliferative capacity of NK cells were determined by Cell Counting Kit-8 (CCK-8) assay. (I–L) After intervening for 24 h of scutellarein (I), lobetyolin (J), icariin (K), and curcumenol (L), flow cytometry analysis was performed to detected the percentage of NKp46$^+$ in NK cells. $^*P < 0.05$ and $^{**}P < 0.01$. ns: not significancet. SSC-A: side scatter-area.

categorized by their functions, but each with its unique feature. TCM formulas are composed of different herbs to generate a holistic approach of medical care and have been proven to be effective in disease treatment. However, developing a standardized treatment requires the identification of components that execute the major function of the formula, namely, enhancing NK cell function and NK cell-mediated ADCC effects in our study. UPLC-QE-MS/MS is an effective method for the rapid and accurate analysis and identification of components in TCM, with ultra-high resolution and sensitivity, specifically suitable for qualitative and quantitative analyses of complex chemical components [62]. In our study, functional validation was conducted to assess the influence of four

distinctive components of XLLXF on NK cell function, revealing the enhancing effect of monomers such as scutellarein on NK cell activity. Taken together, these results point to the antitumor immune capacity and potential mechanisms of XLLXF in HER2-positive BC.

5. Conclusion

Our study demonstrated that XLLXF played a synergistic role in the trastuzumab-targeted treatment of HER2-positive BC. This result was attributed to the enhancement of NK cell activity and the ADCC effect. Additionally, the enhanced tumor-killing ability of NK cells was associated with the downregulation of *CISH* expression and the activation of the JAK1/STAT5 signaling pathway induced by XLLXF. This process was accompanied with an increase in NKp46 and NKG2D expression. In the future, therapeutics that target NK cells and ADCC may offer novel strategies for the trastuzumab-targeted treatment of HER2-positive BC. Our study offers a unique perspective and potential strategy for treating HER2-positive BC.

CRediT author statement

Feifei Li: Methodology, Investigation, Visualization, Writing - Original draft preparation; **Youyang Shi:** Methodology, Formal analysis; **Mei Ma:** Methodology, Investigation, Formal analysis, Visualization; **Xiaojuan Yang:** Methodology, Formal analysis, Supervision; **Xiaosong Chen:** Conceptualization, Writing - Reviewing and editing, Funding acquisition; **Ying Xie:** Methodology, Investigation, Formal analysis, Visualization, Writing - Original draft preparation; **Sheng Liu:** Conceptualization, Resources, Project administration, Writing - Reviewing and Editing, Funding acquisition.

Declaration of competing interest

The authors declare that there are no conflicts of interest.

Acknowledgments

This work was supported by the National Natural Science Foundation of China (Grant No.: 81774308), the Multi-center Clinical Research Project for Major Diseases of Shanghai Shenkang Hospital Development Center, China (Grant No.: SHDC2020CR1050B), and the High-level University Building Innovation Team, China (Grant No.: 601521D).

Appendix A. Supplementary data

Supplementary data to this article can be found online at https://doi.org/10.1016/j.jpha.2024.100977.

References

[1] R.L. Siegel, K.D. Miller, N.S. Wagle, et al., Cancer statistics, 2023, CA Cancer J. Clin. 73 (2023) 17–48.
[2] S. Loibl, L. Gianni, HER2-positive breast cancer, Lancet 389 (2017) 2415–2429.
[3] D.J. Slamon, B. Leyland-Jones, S. Shak, et al., Use of chemotherapy plus a monoclonal antibody against HER2 for metastatic breast cancer that overexpresses HER2, N. Engl. J. Med. 344 (2001) 783–792.
[4] C.S. Wynn, S.C. Tang, Anti-HER2 therapy in metastatic breast cancer: Many choices and future directions, Cancer Metastasis Rev. 41 (2022) 193–209.
[5] K.S. Vega Cano, D.H. Marmolejo Castañeda, S. Escrivá-de-Romaní, et al., Systemic therapy for HER2-positive metastatic breast cancer: Current and future trends, Cancers 15 (2022), 51.
[6] H. Kennecke, R. Yerushalmi, R. Woods, et al., Metastatic behavior of breast cancer subtypes, J. Clin. Oncol. 28 (2010) 3271–3277.
[7] N. Harbeck, C.S. Huang, S. Hurvitz, et al., Afatinib plus vinorelbine versus trastuzumab plus vinorelbine in patients with HER2-overexpressing metastatic breast cancer who had progressed on one previous trastuzumab treatment (LUX-Breast 1): An open-label, randomised, phase 3 trial, Lancet Oncol 17 (2016) 357–366.
[8] G. Nader-Marta, D. Martins-Branco, E. de Azambuja, How we treat patients with metastatic HER2-positive breast cancer, ESMO Open 7 (2022), 100343.
[9] F. Li, S. Liu, Focusing on NK cells and ADCC: A promising immunotherapy approach in targeted therapy for HER2-positive breast cancer, Front. Immunol. 13 (2022), 1083462.
[10] F.A.I. Ehlers, N.A. Beelen, M. van Gelder, et al., ADCC-inducing antibody trastuzumab and selection of KIR-HLA ligand mismatched donors enhance the NK cell anti-breast cancer response, Cancers 13 (2021), 3232.
[11] R. Du, X. Zhang, X. Lu, et al., PDPN positive CAFs contribute to HER2 positive breast cancer resistance to trastuzumab by inhibiting antibody-dependent NK cell-mediated cytotoxicity, Drug Resist. Updat. 68 (2023), 100947.
[12] G.D. Rak, E.M. Mace, P.P. Banerjee, et al., Natural killer cell lytic granule secretion occurs through a pervasive actin network at the immune synapse, PLoS Biol. 9 (2011), e1001151.
[13] X. Ren, M. Peng, P. Xing, et al., Blockade of the immunosuppressive KIR2DL5/PVR pathway elicits potent human NK cell-mediated antitumor immunity, J. Clin. Invest. 132 (2022), e163620.
[14] B. Lipinski, P. Arras, L. Pekar, et al., NKp46-specific single domain antibodies enable facile engineering of various potent NK cell engager formats, Protein Sci. 32 (2023), e4593.
[15] A. Glasner, H. Ghadially, C. Gur, et al., Recognition and prevention of tumor metastasis by the NK receptor NKp46/NCR1, J. Immunol. 188 (2012) 2509–2515.
[16] L. Gauthier, A. Morel, N. Anceriz, et al., Multifunctional natural killer cell engagers targeting NKp46 trigger protective tumor immunity, Cell 177 (2019) 1701–1713.e16.
[17] P. Peng, Y. Lou, S. Wang, et al., Activated NK cells reprogram MDSCs via NKG2D-NKG2DL and IFN-γ to modulate antitumor T-cell response after cryothermal therapy, J. Immunother. Cancer 10 (2022), e005769.
[18] S. Vasu, S. He, C. Cheney, et al., Decitabine enhances anti-CD33 monoclonal antibody BI 836858-mediated natural killer ADCC against AML blasts, Blood 127 (2016) 2879–2889.
[19] J. Xing, S. Liu, X. Tang, et al., Retrospective analysis of HER-2 overexpressing breast cancer treated with breast cancer postoperatively, J. Liaoning U. Tradit, Chin. Med. 24 (2022) 112–120.
[20] G. Chen, Z. Cao, Z. Shi, et al., Microbiome analysis combined with targeted metabolomics reveal immunological anti-tumor activity of icariside I in a melanoma mouse model, Biomed. Pharmacother. 140 (2021), 111542.
[21] L. Song, X. Chen, L. Mi, et al., Icariin-induced inhibition of SIRT6/NF-κB triggers redox mediated apoptosis and enhances anti-tumor immunity in triple-negative breast cancer, Cancer Sci. 111 (2020) 4242–4256.
[22] S. Dandawate, L. Williams, N. Joshee, et al., *Scutellaria* extract and wogonin inhibit tumor-mediated induction of T_{reg} cells via inhibition of TGF-β1 activity, Cancer Immunol. Immunother. 61 (2012) 701–711.
[23] W. Li, Q. Xu, Y. He, et al., Anti-tumor effect of steamed *Codonopsis lanceolata* in H22 tumor-bearing mice and its possible mechanism, Nutrients 7 (2015) 8294–8307.
[24] F. Li, Y. Shi, Y. Zhang, et al., Investigating the mechanism of Xian-Ling-Lian-Xia-Fang for inhibiting vasculogenic mimicry in triple negative breast cancer via blocking VEGF/MMPs pathway, Chin. Med. 17 (2022), 44.
[25] J. Wu, F. Gao, C. Wang, et al., IL-6 and IL-8 secreted by tumour cells impair the function of NK cells via the STAT3 pathway in oesophageal squamous cell carcinoma, J. Exp. Clin. Cancer Res. 38 (2019), 321.
[26] L. Li, T. Liu, L. Shi, et al., HER2-targeted dual radiotracer approach with clinical potential for noninvasive imaging of trastuzumab-resistance caused by epitope masking, Theranostics 12 (2022) 5551–5563.
[27] J. Scerri, C. Scerri, F. Schäfer-Ruoff, et al., PKC-mediated phosphorylation and activation of the MEK/ERK pathway as a mechanism of acquired trastuzumab resistance in HER2-positive breast cancer, Front. Endocrinol. 13 (2022), 1010092.
[28] W. Li, J. Zhou, X. Wang, et al., $CD49a^{+}CD49b^{+}$ NK cells induced by viral infection reflect an activated state of conventional NK cells, Sci, China Life Sci. 63 (2020) 1725–1733.
[29] L. Martinet, M.J. Smyth, Balancing natural killer cell activation through paired receptors, Nat. Rev. Immunol. 15 (2015) 243–254.
[30] M.D. Miljkovic, S.P. Dubois, J.R. Müller, et al., Interleukin-15 augments NK cell-mediated ADCC of alemtuzumab in patients with $CD52^{+}$ T-cell malignancies, Blood Adv 7 (2023) 384–394.
[31] F. Carrette, E. Vivier, NKG2A blocks the anti-metastatic functions of natural killer cells, Cancer Cell 41 (2023) 232–234.
[32] G. Zheng, Z. Guo, W. Li, et al., Interaction between HLA-G and NK cell receptor KIR2DL4 orchestrates HER2-positive breast cancer resistance to trastuzumab, Signal Transduct. Target. Ther. 6 (2021), 236.
[33] J. Yang, A. Kumar, A.E. Vilgelm, et al., Loss of CXCR4 in myeloid cells enhances antitumor immunity and reduces melanoma growth through NK cell and FASL mechanisms, Cancer Immunol. Res. 6 (2018) 1186–1198.
[34] K. Fousek, L.A. Horn, H. Qin, et al., An interleukin-15 superagonist enables antitumor efficacy of natural killer cells against all molecular variants of SCLC, J. Thorac. Oncol. 18 (2023) 350–368.
[35] R.B. Delconte, T.B. Kolesnik, L.F. Dagley, et al., CIS is a potent checkpoint in NK cell-mediated tumor immunity, Nat. Immunol. 17 (2016) 816–824.
[36] H. Zhu, R.H. Blum, D. Bernareggi, et al., Metabolic reprograming via deletion of CISH in human iPSC-derived NK cells promotes *in vivo* persistence and enhances anti-tumor activity, Cell Stem Cell 27 (2020) 224–237.e6.

[37] D. Cameron, M.J. Piccart-Gebhart, R.D. Gelber, et al., 11 years' follow-up of trastuzumab after adjuvant chemotherapy in HER2-positive early breast cancer: Final analysis of the HERceptin adjuvant (HERA) trial, Lancet 389 (2017) 1195–1205.
[38] R. Ghosh, A. Narasanna, S.E. Wang, et al., Trastuzumab has preferential activity against breast cancers driven by HER2 homodimers, Cancer Res. 71 (2011) 1871–1882.
[39] H. Maadi, Z. Wang, A novel mechanism underlying the inhibitory effects of trastuzumab on the growth of HER2-positive breast cancer cells, Cells 11 (2022), 4093.
[40] S. Chumsri, Advancing outcomes of metastatic HER2-positive breast cancer, Lancet 401 (2023) 1746–1747.
[41] M. Shang, Y. Chi, J. Zhang, et al., The therapeutic effectiveness of neoadjuvant trastuzumab plus chemotherapy for HER2-positive breast cancer can be predicted by tumor-infiltrating lymphocytes and PD-L1 expression, Front. Oncol. 11 (2021), 706606.
[42] S. Bruni, F.L. Mauro, C.J. Proietti, et al., Blocking soluble TNFα sensitizes HER2-positive breast cancer to trastuzumab through MUC4 downregulation and subverts immunosuppression, J. Immunother. Cancer 11 (2023), e005325.
[43] F. Meng, S. Zhang, J. Xie, et al., Leveraging CD16 fusion receptors to remodel the immune response for enhancing anti-tumor immunotherapy in iPSC-derived NK cells, J. Hematol. Oncol. 16 (2023), 62.
[44] L. Mecklenburg, B. Tychsen, R. Paus, Learning from nudity: Lessons from the nude phenotype, Exp. Dermatol. 14 (2005) 797–810.
[45] J. Fogh, J.M. Fogh, T. Orfeo, One hundred and twenty-seven cultured human tumor cell lines producing tumors in nude mice, J. Natl. Cancer Inst. 59 (1977) 221–226.
[46] L.D. Shultz, F. Ishikawa, D.L. Greiner, Humanized mice in translational biomedical research, Nat. Rev. Immunol. 7 (2007) 118–130.
[47] I. Szadvari, O. Krizanova, P. Babula, Athymic nude mice as an experimental model for cancer treatment, Physiol. Res. 65 (2016) S441–S453.
[48] J. Lv, L. Qin, R. Zhao, et al., Disruption of CISH promotes the antitumor activity of human T cells and decreases PD-1 expression levels, Mol. Ther. Oncolytics 28 (2023) 46–58.
[49] F. Souza-Fonseca-Guimaraes, G.R. Rossi, L.F. Dagley, et al., TGFβ and CIS inhibition overcomes NK-cell suppression to restore antitumor immunity, Cancer Immunol. Res. 10 (2022) 1047–1054.
[50] J. Bi, C. Huang, X. Jin, et al., TIPE2 deletion improves the therapeutic potential of adoptively transferred NK cells, J. Immunother. Cancer 11 (2023), e006002.
[51] K.M. Maalej, M. Merhi, V.P. Inchakalody, et al., CAR-cell therapy in the era of solid tumor treatment: Current challenges and emerging therapeutic advances, Mol. Cancer 22 (2023), 20.
[52] R. Elahi, A.H. Heidary, K. Hadiloo, et al., Chimeric antigen receptor-engineered natural killer (CAR NK) cells in cancer treatment; recent advances and future prospects, Stem Cell Rev. Rep. 17 (2021) 2081–2106.
[53] H. Ebrahimiyan, A. Tamimi, B. Shokoohian, et al., Novel insights in CAR-NK cells beyond CAR-T cell technology; promising advantages, Int. Immunopharmacol. 106 (2022), 108587.
[54] O. Cienfuegos-Jimenez, E. Vazquez-Garza, A. Rojas-Martinez, CAR-NK cells for cancer therapy: Molecular redesign of the innate antineoplastic response, Curr, Gene Ther 22 (2022) 303–318.
[55] B. Cao, M. Liu, L. Wang, et al., Use of chimeric antigen receptor NK-92 cells to target mesothelin in ovarian cancer, Biochem. Biophys. Res. Commun. 524 (2020) 96–102.
[56] S. Klöß, O. Oberschmidt, M. Morgan, et al., Optimization of human NK cell manufacturing: Fully automated separation, improved *ex vivo* expansion using IL-21 with autologous feeder cells, and generation of anti-CD123-CAR-expressing effector cells, Hum, Gene Ther 28 (2017) 897–913.
[57] J. Tanaka, J.S. Miller, Recent progress in and challenges in cellular therapy using NK cells for hematological malignancies, Blood Rev 44 (2020), 100678.
[58] I. Pedroza-Pacheco, A. Madrigal, A. Saudemont, Interaction between natural killer cells and regulatory T cells: Perspectives for immunotherapy, Cell. Mol. Immunol. 10 (2013) 222–229.
[59] T.A. Waldmann, E. Lugli, M. Roederer, et al., Safety (toxicity), pharmacokinetics, immunogenicity, and impact on elements of the normal immune system of recombinant human IL-15 in rhesus macaques, Blood 117 (2011) 4787–4795.
[60] T. Bald, M.F. Krummel, M.J. Smyth, et al., The NK cell-cancer cycle: Advances and new challenges in NK cell-based immunotherapies, Nat. Immunol. 21 (2020) 835–847.
[61] C. Di Nitto, E. Gilardoni, J. Mock, et al., An engineered IFNγ-antibody fusion protein with improved tumor-homing properties, Pharmaceutics 15 (2023), 377.
[62] Y. Miao, X. Fan, L. Wei, et al., Lizhong decoction ameliorates pulmonary infection secondary to severe traumatic brain injury in rats by regulating the intestinal physical barrier and immune response, J. Ethnopharmacol. 311 (2023), 116346.